



# The mechanistic basis for interprotomer deglycosylation of antibodies by corynebacterial IgG-specific endoglycosidases

Received: 6 February 2025

Accepted: 10 June 2025

Published online: 04 July 2025

Check for updates

Diego E. Sastre <sup>1</sup>✉, Stylianos Bournazos <sup>2</sup>, Maros Huliciak <sup>1</sup>, Barbara Ann C. Grace <sup>2</sup>, E. Josephine Boder <sup>2</sup>, Jonathan Du <sup>1,7</sup>, Nazneen Sultana <sup>1,8</sup>, Tala Azzam <sup>1</sup>, Trenton J. Brown <sup>1</sup>, Maria W. Flowers <sup>1</sup>, Pete Lollar <sup>3</sup>, Ting Xu <sup>1</sup>, Tatiana A. Chernova <sup>1</sup>, Alasdair D. Keith <sup>1</sup>, Meredith Keen <sup>1</sup>, Abigail Saltzman <sup>1</sup>, Ana Martinez Gascueña <sup>4</sup>, Beatriz Trastoy <sup>4,5</sup>, Marcelo E. Guerin <sup>6</sup>, Filipp Frank <sup>1</sup>, Eric A. Ortlund <sup>1</sup>, Jeffrey V. Ravetch <sup>2</sup> & Eric J. Sundberg <sup>1</sup>✉

*Corynebacterium diphtheriae* clade species secrete single-domain endo- $\beta$ -N-acetylglucosaminidases (ENGases) that specifically bind to human IgG antibodies and hydrolyze their N297-linked glycans. Here, we define the molecular mechanisms of IgG-specific deglycosylation for the entire family of corynebacterial IgG-specific ENGases, including but not limited to CU43 and CM49. By solving the crystal structure of CU43 in a 1:1 complex with the IgG1 Fc region, combined with targeted and saturation mutagenesis analysis and activity measurements using engineered antibodies, we establish an interprotomeric mechanism of recognition and deglycosylation of IgG antibodies. Using in silico modeling, small-angle X-ray scattering and saturation mutagenesis we determine that CM49 uses a unique binding site on the Fc region, to process N297-linked glycans. Moreover, we demonstrate that CU43 treatment is highly effective in abrogating Fc effector functions in humanized mouse models, while preserving the neutralizing capacity of anti-influenza IgG antibodies, thereby conferring protection against lethal influenza challenge.

Nearly all Endo- $\beta$ -N-acetylglucosaminidases (endoglycosidases, ENGases) recognize and hydrolyze the  $\beta$ -1,4 linkage between the first two N-acetylglucosamine (GlcNAc) saccharides of asparagine-linked glycans on their glycoprotein substrates (EC 3.2.1.96) strictly through glycan-specific mechanisms<sup>1-4</sup>. However, there exist rare ENGases that

hydrolyze only the N297-linked glycan on the fragment crystallizable (Fc) region of IgG antibodies<sup>5</sup>. This glycan serves as the major molecular determinant for Fc  $\gamma$  receptor (Fc $\gamma$ R) binding and its presence and chemical composition dictate antibody-mediated effector functions<sup>6,7</sup>. Consequently, the activity of IgG-specific ENGases

<sup>1</sup>Department of Biochemistry, Emory University School of Medicine, Atlanta, GA, USA. <sup>2</sup>Laboratory of Molecular Genetics and Immunology, The Rockefeller University, New York, NY, USA. <sup>3</sup>Department of Pediatrics, Emory University School of Medicine, Atlanta, GA, USA. <sup>4</sup>Structural Glycoimmunology Laboratory, Biobizkaia Health Research Institute, Barakaldo, Bizkaia, Spain. <sup>5</sup>Ikerbasque, Basque Foundation for Science, Bilbao, Spain. <sup>6</sup>Structural Glycobiology Laboratory, Department of Structural and Molecular Biology; Molecular Biology Institute of Barcelona (IBMB), CSIC, Barcelona Science Park, c/Baldíri Reixac 4-8, Tower R, Barcelona, Catalonia, Spain. <sup>7</sup>Present address: Sydney Pharmacy School, Faculty of Medicine and Health, The University of Sydney, Camperdown, NSW, Australia. <sup>8</sup>Present address: Structural Biochemistry Unit, National Institute of Dental and Craniofacial Research (NIDCR)/National Institute of Health, Bethesda, MD, USA. ✉e-mail: [dsastre@emory.edu](mailto:dsastre@emory.edu); [eric.sundberg@emory.edu](mailto:eric.sundberg@emory.edu)

suppresses the immune response and, thus, some pathogenic bacteria secrete these IgG-specific ENGases to evade the host immune response, enhancing bacterial survival and virulence<sup>8</sup>.

We previously defined the structural determinants governing *N*-glycan specificities of the streptococcal multi-domain IgG-specific ENGases EndoS, which hydrolyzes only biantennary complex-type *N*-glycans, and EndoS2, which hydrolyzes complex-type, hybrid and high-mannose *N*-glycans<sup>9–11</sup>. We and others have also described the molecular mechanism of recognition and specificity by EndoS and EndoS2 for IgG antibodies, revealing how these enzymes exclusively process the *N*-glycan on the Fc region of IgG. These studies also highlighted the requirement of a non-enzymatic  $\beta$ -sandwich domain to create an anchor point on the IgG substrate by forming a protein–protein interaction<sup>10–14</sup>.

*Corynebacterium pseudotuberculosis* secretes CP40, a 40 kDa protein identified as a protective antigen against ovine caseous lymphadenitis that was erroneously described as a serine protease<sup>15</sup> but subsequently characterized as an ENGase capable of hydrolyzing *N*-glycans on human IgG antibodies<sup>16</sup>. More recently, we identified a family of single-domain ENGases secreted by different pathogenic corynebacterial species that exhibit strict specificity for the N297-linked glycan on human IgG antibodies, including CP40. We demonstrated potent *in vivo* efficacy of a prototypical member of this IgG-specific ENGase family, known as CU43, in mitigating diverse pathologies that rely on IgG-mediated effector functions, including the prevention of CD4+ T cell and B cell depletion, autoimmune hemolytic anemia, and antibody-dependent enhancement in severe dengue disease<sup>17</sup>. However, the precise molecular mechanism by which corynebacterial IgG-specific ENGases hydrolyze *N*-glycans exclusively on IgG antibody substrates is yet unknown.

In this work, we unveil the catalytic mechanisms of the entire family of IgG-specific ENGases secreted by pathogenic corynebacterial species with strict specificity for deglycosylation of human IgG antibodies. We show that these ENGases can be further classified into subfamilies, each of which exhibits a distinct molecular mechanism of action. Additionally, we show that CU43 deglycosylates IgG antibodies through an inter-protomer mechanism by binding to one Fc protomer to hydrolyze the N297-linked glycan on the opposite Fc protomer, contrasting the intra-protomer deglycosylation mechanism employed by the Streptococcal IgG-specific ENGases. Finally, we demonstrate in a humanized mouse model of lethal influenza infection that IgG deglycosylation by CU43 preserves the protective neutralization capacity of an anti-flu broadly neutralizing antibody, unlike the IgG degrader therapeutic Efgartigimod. Our insights into the molecular mechanisms by which corynebacterial IgG-specific ENGases hydrolyze Fc glycans will guide their development as therapeutics for antibody-mediated diseases in humans.

## Results

### CU43 forms a complex with the Fc region with 1:1 stoichiometry

We previously showed that the single-domain IgG-specific ENGase CU43 (Fig. 1a) is able to interact specifically with both protein and glycan components of the Fc region human IgG antibodies and that it could bind to aglycosylated IgG, indicative of a direct protein–protein interaction between CU43 and Fc<sup>17</sup>. In order to evaluate the formation of a protein complex between CU43 and Fc and its stoichiometry, we incubated catalytically-inactive CU43 (CU43i, containing a D187A–E189A double mutation to abolish hydrolytic activity) with the Fc region of human IgG1 (with biantennary complex-type (CT) *N*-glycans linked to N297) in a 2:1 (CU43i:Fc) molar ratio and evaluated complex formation by size exclusion chromatography (SEC; Supplementary Fig. 1a and Supplementary Table 1) and SEC-multiple angle light scattering (MALS; Fig. 1b). As shown in Fig. 1b, we observed the formation of a 1:1 CU43i:Fc-CT complex; SDS-PAGE analysis of the SEC column fractions clearly showed the co-elution of CU43 and Fc. We validated

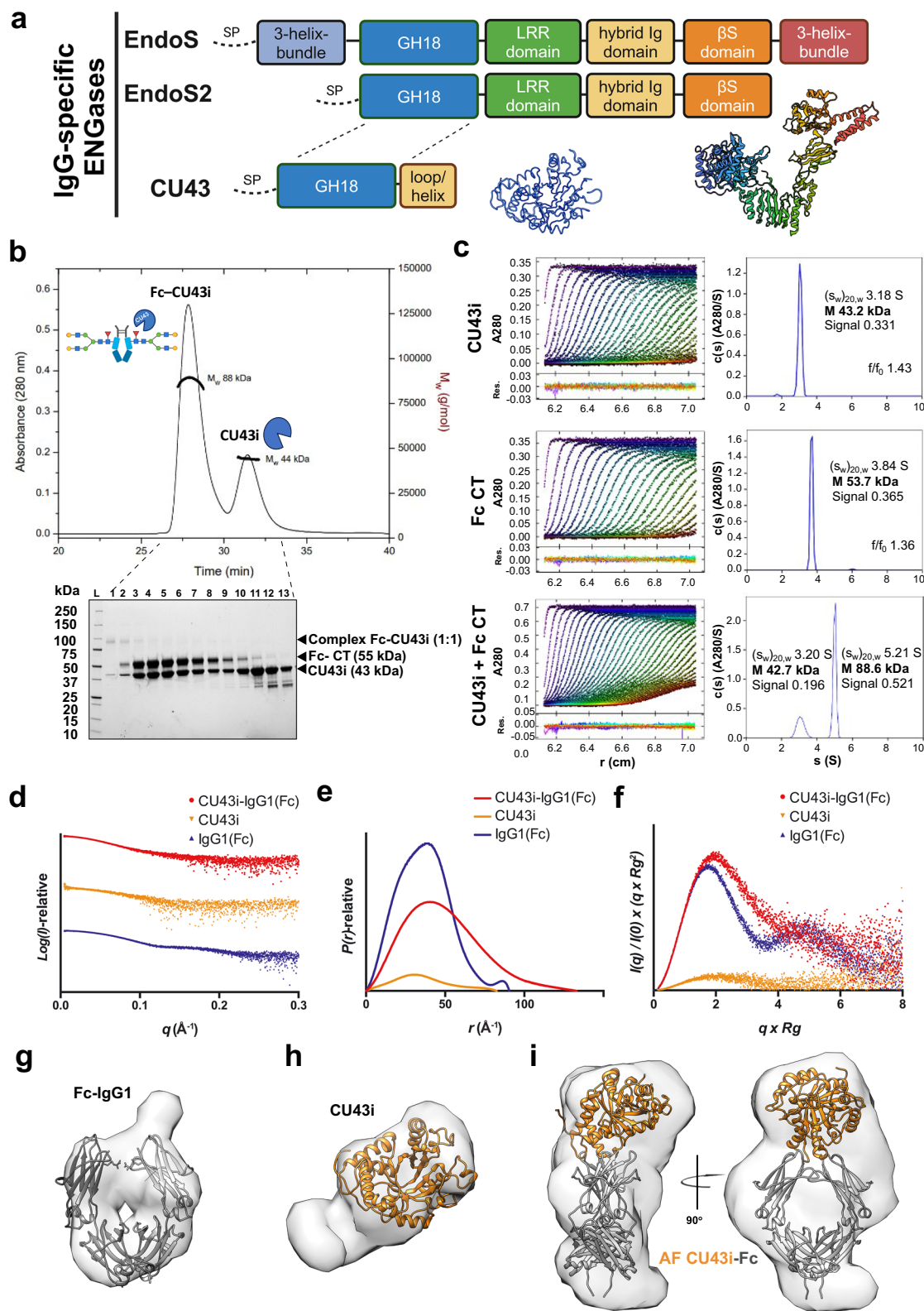
the 1:1 stoichiometry of the CU43-Fc complex by mass photometry (Supplementary Fig. 1b) and analytical ultracentrifugation (AUC) (Fig. 1c). Using these techniques, we estimated molecular weight of the CU43i-Fc complex of 88–93 kDa, similar to the 98 kDa predicted by combining the amino acid sequences of the individual proteins. Overall, these data are consistent with the binding of CU43i to Fc at a ratio of one CU43i molecule per Fc dimer. We also performed small-angle X-ray scattering (SAXS) with in-line SEC (Fig. 1d–f, Supplementary Table 1) and reconstructed ab initio envelopes for Fc region (Fig. 1g), CU43i (Fig. 1h) and the CU43i:Fc-CT complex (Fig. 1i). For the complex, we calculated a molecular weight of 99.9 kDa and fitted an AlphaFold3 (AF3) model of the CU43i-Fc complex into the SAXS envelope (Fig. 1j).

### Structural basis of IgG-specific deglycosylation by CU43

We combined CU43i in a 1:1 molar ratio with the E382S IgG1 Fc variant that disfavors crystal packing interactions that would lead to Fc self-crystallization<sup>12</sup>, purified the resulting complex by SEC (Supplementary Fig. 1a) and obtained crystals of the CU43i-Fc<sup>E382S</sup> complex. We determined the structure by molecular replacement methods, using CU43i (PDB code: 8UEN) and Fc region (PDB code: 5JLH) structures as search models, to an overall resolution of 3.6 Å (Supplementary Table 2). In the structure of the CU43i-Fc<sup>E382S</sup> complex, CU43i binds to one protomer of the Fc region by forming a protein–protein interface with residues from the top of the CH2 domain of that Fc protomer, as well as those in the lower hinge region (Fig. 2a). In this binding mode, CU43i engages the Fc homodimer asymmetrically, positioned to deglycosylate the Fc protomer opposite to which it binds by what would be an inter-protomer mechanism glycan hydrolysis (Fig. 2b). Docking of the *N*-glycan GOF into the protein structure was performed to facilitate mechanistic interpretation (Fig. 2a–b). The 1:1 stoichiometry of the CU43i:Fc<sup>E382S</sup> homodimer that we observed in the crystal structure is consistent with our AUC, SEC-MALS, SEC-SAXS and mass photometry analyses (Fig. 1 and Supplementary Fig. 1b). Throughout our crystal structure, the electron density is heterogeneous. We observed unambiguous electron density for the entire CU43i molecule, the entire Fc protomer to which it forms a protein–protein interface (involving FG-loop residues from Fc and at least six residues of CU43 located less than 4 Å apart) (Fig. 2a–c and Supplementary Fig. 2), as well as the opposite Fc protomer from its C-terminus through the interface between its CH2 and CH3 domains. The electron density gets increasingly less interpretable through the CH2 domain of the unbound Fc protomer. The quality of the electron density is reflected in the crystallographic B-factors throughout the structure of the CU43i-Fc<sup>E382S</sup> complex (Fig. 2d), likely attributable to the high solvent content in the crystal (~65%) and the crystal packing that could allow asymmetrical flexibility of Fc protomers (Supplementary Fig. 3). We were able to fit the CU43i-Fc complex structure in the SAXS envelope, indicating that the low-resolution ab-initio structure obtained in solution is in clear agreement with the crystal structure (Supplementary Fig. 4). Analysis of the electrostatic potential of the solvent accessible molecular surfaces of both CU43i and the Fc region reveals that a highly positively charged patch on the CU43i surface is juxtaposed to the highly negatively charged tip of the CH2 region of the bound Fc protomer to form the protein–protein interface (Fig. 2e), suggesting that CU43i engages the Fc region by an electrostatic steering mechanism. Indeed, using mass photometry, we found the formation of CU43i-Fc<sup>E382S</sup> complex to be highly sensitive to high salt concentrations (Supplementary Fig. 5).

### Targeted and saturation mutagenesis corroborates the IgG-specific deglycosylation mechanism of CU43

To test whether protein–protein and protein–glycan interactions contribute to the enzymatic activity of CU43, we mutated key residues at both CU43 and the Fc region, individually or in combination, and measured the enzymatic activities of the resulting variants (Fig. 3a and



Supplementary Fig. 6). This mutagenesis analysis corroborates the protein-protein and glycan binding site interfaces of the CU43-Fc complex and indicates that the CU43i-Fc<sup>E382S</sup> protein-protein interface observed in the crystal structure is critical for the enzymatic activity of CU43. In particular, mutation to alanine of the CU43 residues 44-SPGQ-47 or R200-W201-R204, which make direct protein-protein contacts to the FG loop of the CH2 domain of the Fc region based on the crystal structure, results in complete abolishment of catalytic

activity. Mutations to glycine in the stretch of residues 325-NKALPAP-331 in the FG-loop of the CH2 domain of the Fc region likewise result in the complete loss of enzymatic activity (Fig. 3a and Supplementary Fig. 6).

We previously reported that wild type CU43 but not CU43i, formulated as an Fc<sup>N297A</sup> fusion protein, could protect mice humanized for Fc $\gamma$  receptors (Fc $\gamma$ Rs) from the mAb-mediated mAb; YTS191 cytotoxic depletion of CD4+ T cells by defeating mAb Fc effector functions<sup>17</sup>. In order to validate the biological relevance of CU43 residues that we

**Fig. 1 | Corynebacterial IgG-specific CU43 forms a complex with Fc with 1:1 stoichiometry.** **a** Schematic representation of domain architecture of IgG-specific ENGases (EndoS, EndoS2) and corynebacterial ENGase CU43. SP=signal peptide. **b** SEC-MALS analysis of CU43i-Fc complex in 2:1 molar ratio (upper panel) and the indicated fractions from SEC were loaded into SDS-PAGE in non-reducing (NR) conditions. Assays were performed in two independent replicates, and consistent results were observed. Blue squares represent GlcNAc, red triangles represent Fucose, Green circles represent Mannose and yellow circles represent Galactose. **c** AUC analysis of CU43i, Fc CT and CU43-Fc 1:1 complex. Samples in PBS were centrifuged at 45,400 xg. Curves represent fits to the continuous c(s) distribution model in SEDFIT. Res.=residuals. **d** SAXS scattering curve of CU43i,

Fc-IgG1 and CU43i-Fc. **e**  $\rho(r)$  functions distributions of CU43i, Fc-IgG1 and CU43i-Fc complex. **f** Normalized Kratky plot CU43i, Fc-IgG1 and CU43i-Fc complex. **g** Ab initio modeling with GASBOR of the envelope of CU43i and superimposition of CU43i (PDB code: 8URA) crystal structure. **h** Ab initio modeling with GASBOR of the envelope of IgG1(Fc) and superimposition of Fc-IgG1 X-ray crystal structure (PDB code: 1H3X). **i** Ab initio modeling with GASBOR of the envelope of CU43i-Fc and superimposition of AF3 CU43i (orange)-Fc (gray) complex predicted model. Schematic figures in panels 1a and 1b were created in BioRender. Sastre, D. (<https://Biorender.com/8gujq6o>) and Sastre, D. (<https://Biorender.com/uh09kf7>) respectively. Source data are provided as a Source Data file.

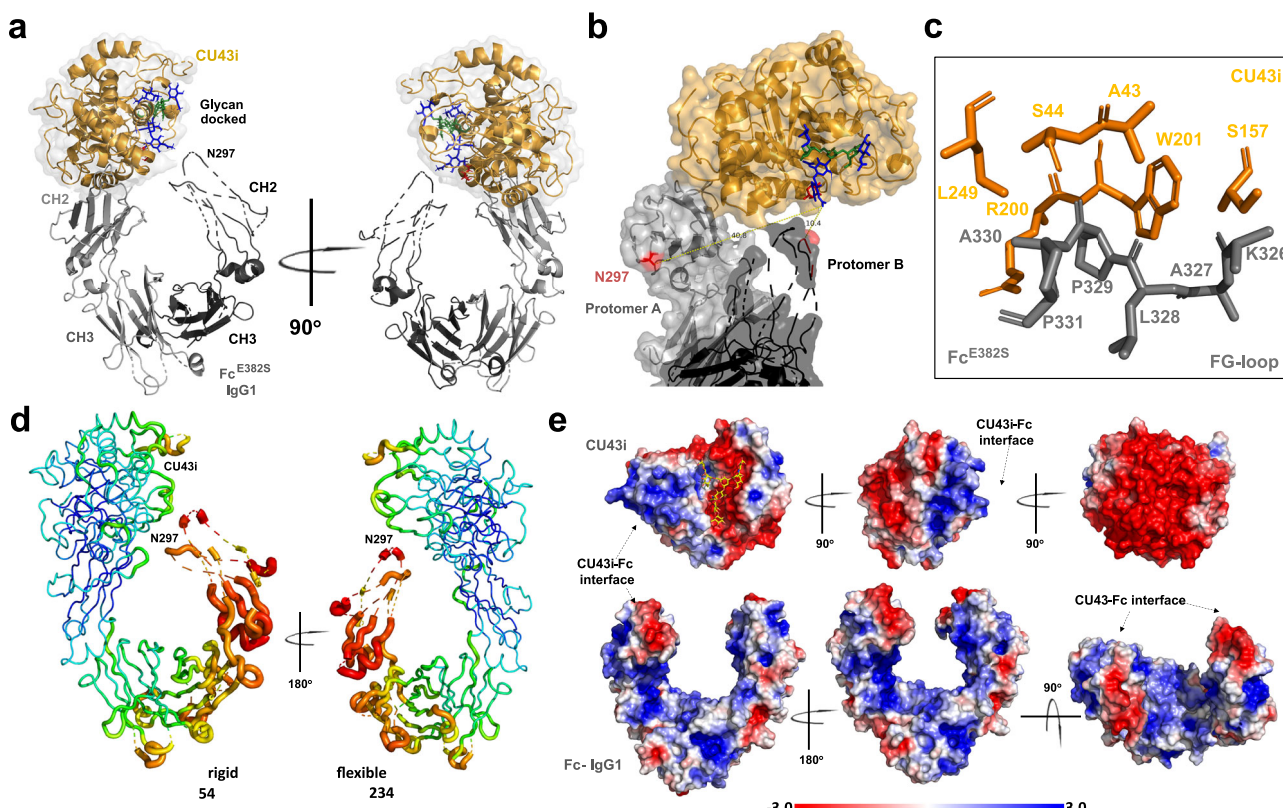


**Fig. 2 | Structural basis of human IgG-specific deglycosylation by CU43.** **a** Two views of cartoon representation of the crystal structure of CU43i-Fc<sup>E382S</sup> crystal structure at 3.6 Å resolution (PDB code: 8URO). GOF N-glycan was docked into CU43i. **b** Surface representation of CU43i-Fc<sup>E382S</sup> with glycan docked showing the distance to N297 from each Fc protomer. **c** Deep view of protein-protein interface

residues of CU43i and Fc<sup>E382S</sup> complex represented as sticks. **d** Two views of crystal structure of CU43i-Fc<sup>E382S</sup> complex representing B-factor values. **e** Surface electrostatic potential of CU43 and Fc IgG1 obtained using (<https://server.poissonboltzmann.org/pdb2pq>). N-glycan GOF was docked in CU43i structure.

identified above to be important for hydrolytic activity (Fig. 3a-c), we employed this humanized mouse model to test the role of these mutations *in vivo*. As shown in Fig. 3d, wild type CU43 prevented the depletion of CD4+T cells, while CU43 mutant variants incapable of binding the IgG N297-linked glycan, including CU43<sup>E260A-Y262A</sup> which recognizes the glycan core, and CU43<sup>E294A-E295A</sup> which recognizes the  $\alpha$ 1-3 branch, were completely incapable of preventing CD4+T cell depletion. Likewise, the CU43<sup>R200A-W201A-R204A</sup> variant which abolishes CU43 protein-protein interactions with the Fc substrate, exhibited no prevention of CD4+T cell depletion. These data corroborate our *in vitro* structural and mutagenesis analyses and demonstrate that CU43 requires both glycan and protein binding to deglycosylate IgG antibodies *in vivo* (Fig. 3d and Supplementary Fig. 7).

To gain deeper insight into how mutations at the Fc region could affect CU43 recognition of its substrate, we employed a site-saturation library of IgG1 Fc variants that included a near-comprehensive set of all possible single-site mutations at each Fc position displayed on the surface of HEK293T cells<sup>18</sup>. We then bound fluorescently-labeled CU43i

to these cells and used fluorescence-activated cell sorting (FACS) to isolate the Fc site-saturation library mutants that exhibited tighter and weaker binding to CU43i. Fc mutations that resulted in substantially reduced binding to CU43i map to the protein and glycan interfaces identified in our CU43i-Fc crystal structure and corroborated our alanine scanning mutagenesis analysis, showing that the lower the binding to Fc, the lower enzymatic activity levels of CU43 (Fig. 4a-c and Supplementary Fig. 8). Moreover, using the same Fc site-saturation library mutants we analyzed the binding of the multi-domain IgG-specific ENGase, EndoS2. As shown in Fig. 4d-f, the pattern of Fc binding to EndoS2 is in complete agreement with the crystal structure of this protein complex (PDB code: 8Q5U<sup>13</sup>), in which the protein-protein binding site is mainly located in the elbow of the CH2 and CH3 domains, clearly distinct from the pattern obtained for CU43 binding to Fc (Fig. 4a-c). Interestingly, the tighter binding mutants in the deep mutagenesis scanning heatmaps were around the glycan loop and neighboring regions, in both CU43i-Fc and EndoS2-Fc complexes (Fig. 4b-e). This was also noticed in the alanine scanning mutagenesis

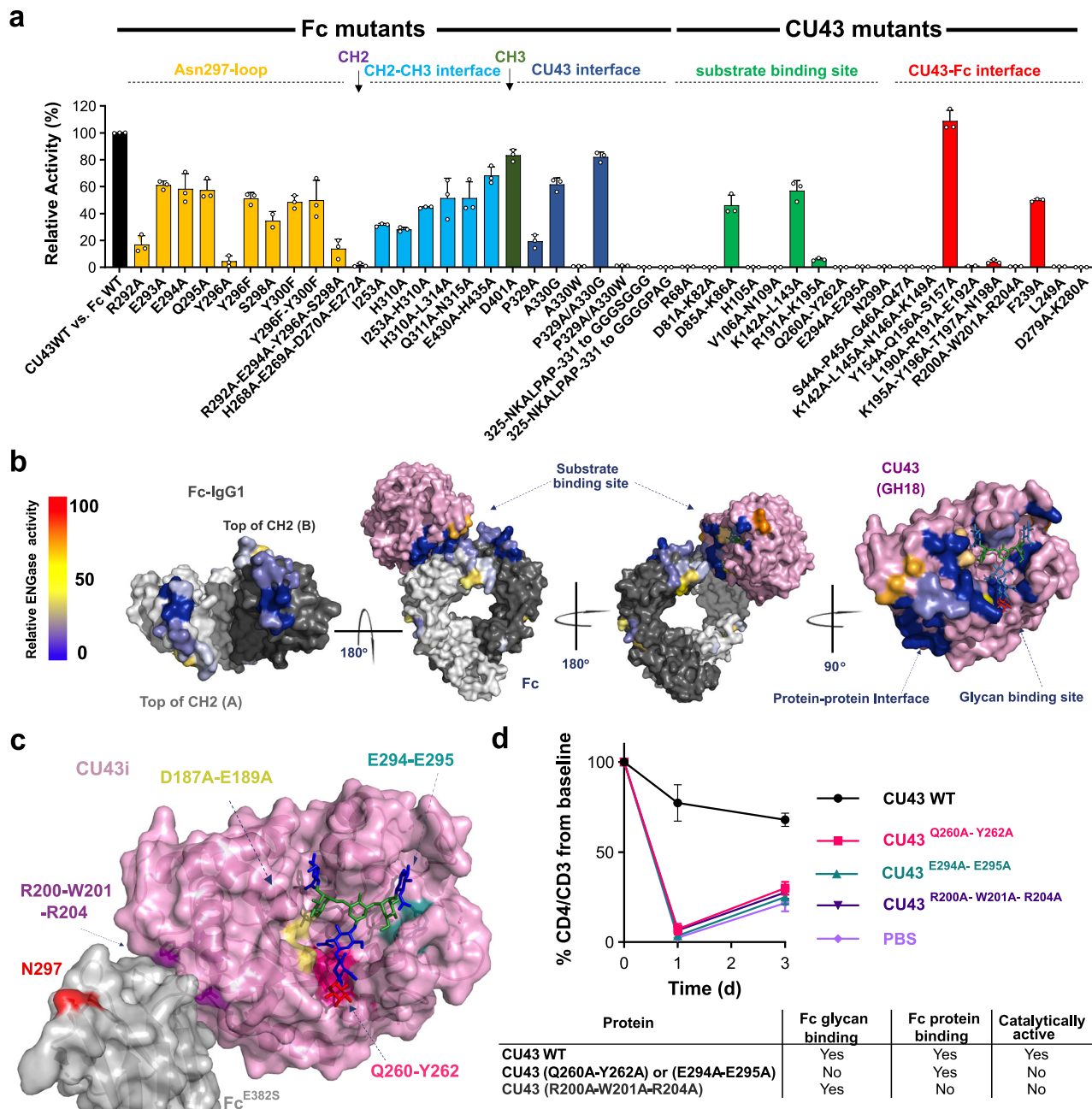
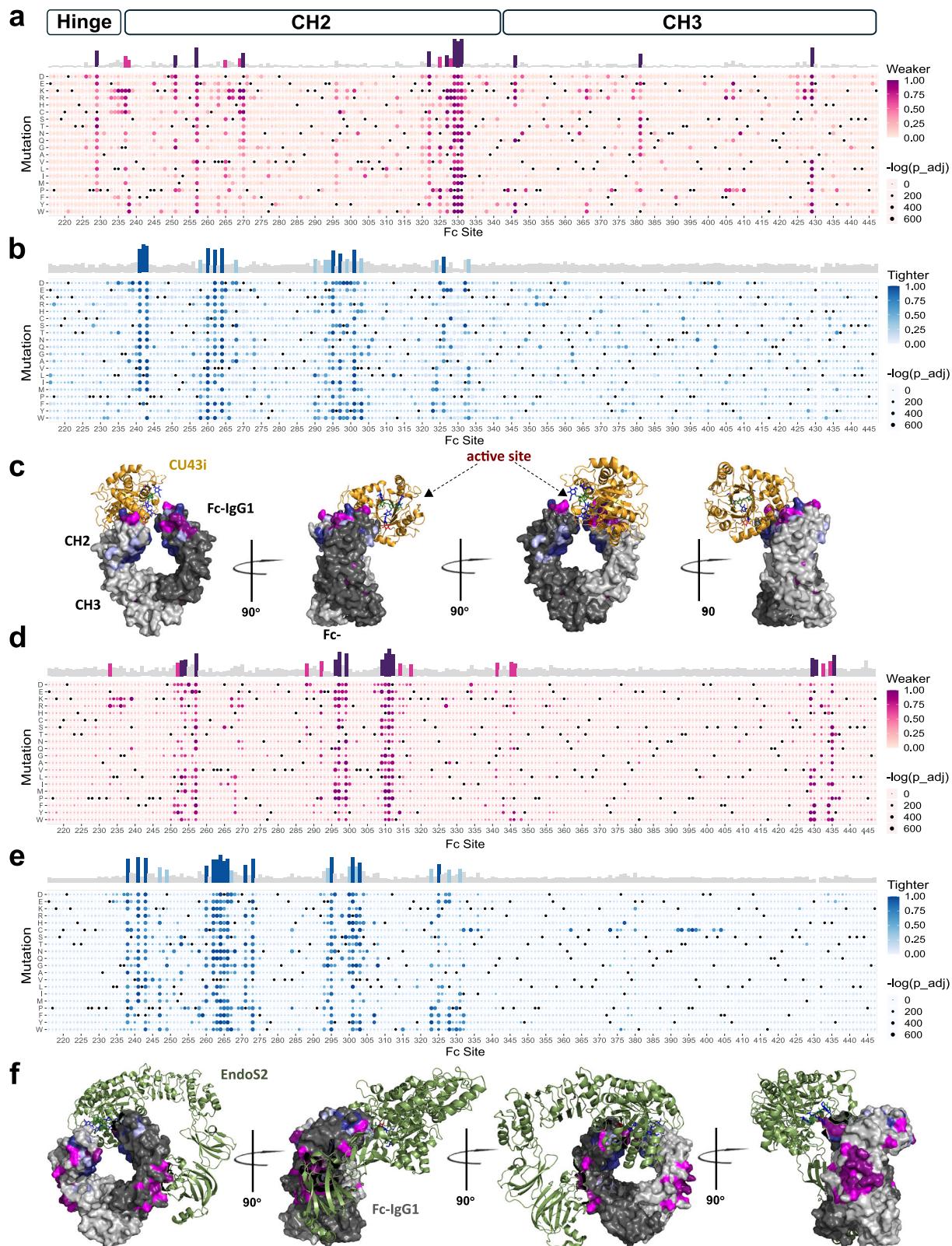


**Fig. 3 | Targeted mutagenesis corroborates the IgG-specific deglycosylation mechanism of CU43. a** ENGase activity of CU43 WT and mutant variants against Fc WT or Fc mutant variants. Incubation of CU43 WT against Fc WT was considered 100 % of activity (1:500 enzyme:substrate molar ratio). Data is presented as mean values from independent samples  $\pm$  SD ( $n = 3$ ). Mean values were obtained by globally fitting the different kinetic traces data using Kintek Global Kinetic Explorer<sup>43</sup>. **b** Surface representation of CU43i-Fc structure color-coded according to the relative activity of each mutant variant from panel A. Protomer B on CU43-Fc<sup>E382S</sup> structure was replaced for a copy of Fc from PDB (code: 5J1H) to show all mutated residues. *N*-glycan GOF was docked into CU43i structure. **c** Surface representation of CU43 and Fc (protomer A) with a GOF glycan docked, in which are colored the key residues involved in the protein-protein interface of CU43 with Fc and the residues involved in the glycan binding site that were used in the *in vivo*

assays indicated in **d**. GlcNAc is colored in blue, Fucose in red and Mannose in green. **d** Validation of CU43-Fc alanine scanning *in vivo*. CU43 WT and mutant variants were fused to Fc<sup>N297A</sup> (CU43 WT-Fc<sup>N297A</sup>, CU43<sup>Q260A-Y262A</sup>-Fc<sup>N297A</sup>, CU43<sup>E294A-E295A</sup>-Fc<sup>N297A</sup>, CU43<sup>R200A-W201A-R204A</sup>-Fc<sup>N297A</sup>) were administered i.v. into Fc $\gamma$ R humanized mice ( $n = 4$ –5/group) follows: CU43 WT 0.5  $\mu$ g/mouse (i.v.) + YTS191 (aCD4) 10  $\mu$ g/mouse (i.v.), CU43<sup>Q260A-E295A</sup> 0.5  $\mu$ g/mouse (i.v.) + YTS191 (aCD4) 10  $\mu$ g/mouse (i.v.), CU43<sup>E294A-E295A</sup> 0.5  $\mu$ g/mouse (i.v.) + YTS191 (aCD4) 10  $\mu$ g/mouse (i.v.), CU43<sup>R200A-W201A-R204A</sup> 0.5  $\mu$ g/mouse (i.v.) + YTS191 (aCD4) 10  $\mu$ g/mouse (i.v.), PBS (i.v.) + YTS191 10  $\mu$ g/mouse (i.v.). The levels of CD4 + T cells in the blood were determined by flow cytometry on days 0, 1, and 3. Results are presented as the mean  $\pm$  SEM from two independent experiments ( $n = 4$ –5 mice/group). Source data are provided as a Source Data file.

analysis of Fc against EndoS<sup>11</sup>, where some of these Fc mutations were more efficiently processed by EndoS compare to Fc WT, suggesting that maybe glycan loop could play some role in Fc protein flexibility and solvent exposure.

**CU43 hydrolyzes IgG glycans by an inter-protomer mechanism**  
Our CU43i-Fc<sup>E382S</sup> crystal structure (Fig. 2) suggests that CU43 binds to one Fc protomer in order to hydrolyze the glycan on the opposite Fc protomer; an inter-protomer mechanism of IgG deglycosylation. To validate this mechanism, we engineered an Fc heterodimer in which



both Fc protomers were glycosylated but only one protomer harbored an A330W mutation, which we had found by both targeted and saturation mutagenesis to abolish CU43 catalytic activity and binding to Fc (Figs. 3a, 4b and 5a–d). We hypothesized that wild type CU43 would be unable to interact with the mutated A330W protomer, leading to the production of monoglycosylated IgG variants. As confirmed by mass spectrometry analysis (Fig. 5e–f), only

monoglycosylated IgG species were obtained following CU43 treatment. Furthermore, to determine which of the two protomers contained the *N*-glycan on the mono-glycosylated product obtained using heterodimeric A330W/WT IgG antibody as the substrate, we treated the IgG with the IgG-specific peptidase IdeS to liberate the two Fc protomers, followed by treatment with the exo-galactosidase BgaA to trim galactose monosaccharides from the N297-linked CT glycan, and

**Fig. 4 | Saturation mutagenesis on Fc corroborates the CU43i-Fc<sup>E382S</sup> glycan structure.** **a** Heatmaps of deep mutational scanning results for IgG1 Fc mutants with **(a)** weaker and **(b)** tighter binding to CU43i. Average weaker/tighter binding scores per site are depicted as bar charts above the heatmaps, with sites highlighted if the score exceeds one (light blue/pink) or two (dark blue/magenta) standard deviations above the mean. **c** Average weaker (magenta/pink) and tighter (dark/light blue) binding scores, color-coded according to the threshold values described in **(a–b)**, mapped onto Fc dimer structure with CU43i depicted in orange. *N*-glycan GOF glycan was docked in CU43i structure. **d–e** Heatmaps of deep mutational

scanning results for IgG1 Fc mutants with **(d)** weaker and **(e)** tighter binding to EndoS2i. Average weaker/tighter binding scores per site are depicted as bar charts above the heatmaps, with sites highlighted if the score exceeds one (light blue/pink) or two (dark blue/magenta) standard deviations above the mean. **f** Average weaker (magenta/pink) and tighter (dark/light blue) binding scores, color-coded according to the threshold values described in **(d, e)**, mapped onto Fc dimer structure with EndoS2i depicted in green. For statistical analysis of DMS data, we used two-sided Fisher's exact test, followed by Bonferroni correction.

then analyzed the resulting products by LC-MS. As shown in Fig. 5g, the N297-linked glycan was absent in the A330W-mutated Fc protomer but present in the non-mutated (wild type) Fc protomer, as shown by the respective masses of each Fc protomer. As a control, we performed the same assay using EndoS2, in which we detected only fully deglycosylated Fc protomers after IdeS/BgaA treatment, indicating that the A330W mutation only affects CU43 binding/activity to Fc but does not affect EndoS2 (Fig. 5h). This data confirms that CU43 employs an inter-protomer mechanism for deglycosylating its IgG substrate in which it makes direct contact with the top of the CH2 domain of one protomer and hydrolyzes the *N*-glycans linked to N297 on the opposite protomer.

#### CU43 decouples the effector functions and neutralization capacities of IgG antibodies

To determine whether excess of non-pathogenic human IgG antibodies could compete with the activity of CU43 against pathogenic antibodies in vivo, we assessed the ability of CU43-Fc to block CD4+ T cell depletion in mice humanized for FcγRs following administration (10 µg, i.v.) of the chimeric rat anti-mouse CD4 mAb YTS191 expressed as human IgG1 (afucosylated) in the presence of intravenous immunoglobulins (IVIG, 5 mg). IVIG could potentially compete with IgG YTS191 for CU43-mediated Fc *N*-glycan cleavage. However, CU43-Fc still exhibited potent activity at 1 µg/mouse to abrogate antibody-effector functions in vivo and to effectively deglycosylate pathogenic as well as excess (5 mg) of non-pathogenic IgGs (Fig. 6a and Supplementary Fig. 9a–b). Furthermore, while a major limitation of neonatal Fc receptor (FcRn)-blocking therapeutics, such as Efgartigimod, is that they reduce the levels of total IgGs, likely leading to immunosuppressive consequences. We hypothesized that CU43 activity only affects glycosylation of antibodies and its effector function without altering the levels of IgGs and their neutralization capacities. To address this hypothesis, we compared the in vivo activity of a neutralizing anti-HA mAb to protect FcγR humanized mice against influenza virus challenge following treatment with CU43 or Efgartigimod. After treatment of FcγR humanized mice with CU43-Fc or Efgartigimod along with the neutralizing monoclonal antibodies recognizing the head of hemagglutinin (HA; anti-HA head mAb 7B2) one day prior to lethal challenge with the H1N1 strain of influenza (Neth/09) (Fig. 6b), we observed that in mice treated with CU43-Fc, 7B2 retained its full neutralization capacity and protected mice from weight loss and mortality (Fig. 6c–e). Conversely, in mice administered Efgartigimod, which indiscriminately accelerates IgG catabolism, 7B2 neutralization capacity was reduced, resulting in significant weight loss and consequently, reduced survival (Fig. 6b–e). Thus, despite both CU43-Fc and Efgartigimod being able to prevent mAb-mediated cytotoxicity in vivo<sup>17</sup>, CU43-Fc hydrolyzes the Fc-associated *N*-glycan to prevent Fc-FcγR interactions but has no effect in the neutralization capacity of IgG antibodies. CU43 effectively decouples the antibody-mediated effector functions and neutralization capacities of IgG antibodies, whereas Efgartigimod, which targets the FcRn pathway to accelerate IgG catabolism,

simultaneously abrogates both antibody effector functions and neutralization (Fig. 6f).

#### CM49 targets a unique binding site on the Fc region to deglycosylate IgG antibodies

To ascertain whether all members of the corynebacterial IgG-specific ENGase family share a similar mechanism of recognition and deglycosylation of N297-linked IgG glycans, we generated molecular models of representative corynebacterial IgG specific ENGases in complex with Fc using AlphaFold3 (AF3)<sup>19</sup> (Supplementary Fig. 10). Most of the corynebacterial IgG-specific ENGases display an Fc binding mode similar to that of CU43, with a per-residue confidence metric called predicted local distance difference test (pLDDT)<sup>20,21</sup> of around 80–85 range, indicating that all ENGase-Fc complexes were predicted confidently (Supplementary Fig. 10); the position of CU43 on the complex with-Fc observed in the AF3 model is in agreement with our CU43i-Fc crystal structure (RMSD = 4.6 Å; average TM-score = 0.55) (Fig. 2a). An AF3 model of CP258 was in closer agreement with our CU43i-Fc<sup>E382S</sup> crystal structure, with an RMSD of 4.3 Å (average TM-score = 0.79) and the Asn297-linked *N*-glycan (GOF) from the opposite Fc protomer appeared optimally positioned in the enzymatic active site (Supplementary Fig. 10b). However, the CM49-Fc model was an exception (Fig. 7a), suggesting that CM49 recognizes the IgG substrate in a manner different from CU43 to hydrolyze N297-linked glycans. Accordingly, we identified two potentially distinct Fc binding modes by corynebacterial ENGases in agreement with the phylogenetic relationships of the individual members of this larger IgG-specific ENGase family (Fig. 7b). CU43 forms a subgroup with five other orthologs, while CM49 forms a phylogenetically distant subgroup together with Csp50 (Fig. 7b), a newly identified protein from *Corynebacterium sp.* (NCBI ID: WP\_303197466.1) that we named Csp50 based on its origin and molecular weight (Supplementary Table 4). This protein shares 83% sequence identity with CM49 and exhibited similar activity and potential binding site on the Fc region as predicted by AF3 (pLDDT=83.2; Supplementary Fig. 10). To validate these predictions, we employed our IgG1 Fc site-saturation mutant library, incubating with fluorescently-labeled catalytically-inactive CM49 (CM49<sup>D171A-E173A</sup> or CM49i) to sort Fc mutants that exhibited tighter and weaker binding (Fig. 7c–e). Indeed, these data corroborate the AF3 model of CM49-Fc and indicate that CM49 engages the Fc region at a site formed by both the CH2 and CH3 domains. We also performed small-angle X-ray scattering (SAXS) with in-line SEC (Fig. 7f–h and Supplementary Table 1) and reconstructed ab initio envelopes for CM49i (Fig. 7i) and the CM49i-Fc complex (Fig. 7j). As shown in Fig. 7j, an AF3 model of the CM49i-Fc complex was validated by its correct fitting into the SAXS envelope despite exhibiting some degree of protein flexibility (Fig. 7j). In contrast to the shared Fc binding site for ProteinA (PDB code: 5U4Y<sup>22</sup>), Protein G (PDB code: 1FCC<sup>23</sup>), FcRn (PDB code: 7Q15<sup>24</sup>), TRIM 21 (PDB code: 2IWG<sup>25</sup>) and β-sandwich (BS) domain of EndoS (PDB code: 8A64<sup>12</sup>), which all bind to the outside surface of the CH2-CH3 elbow, CM49 binds to the inside surface of the CH2-CH3 elbow, where no other Fc-binding protein or enzyme is known to bind (Fig. 8). Moreover, based on deep mutagenesis scanning results, we constructed an Fc with three mutations (K338W-G341R-P343F) in the inner

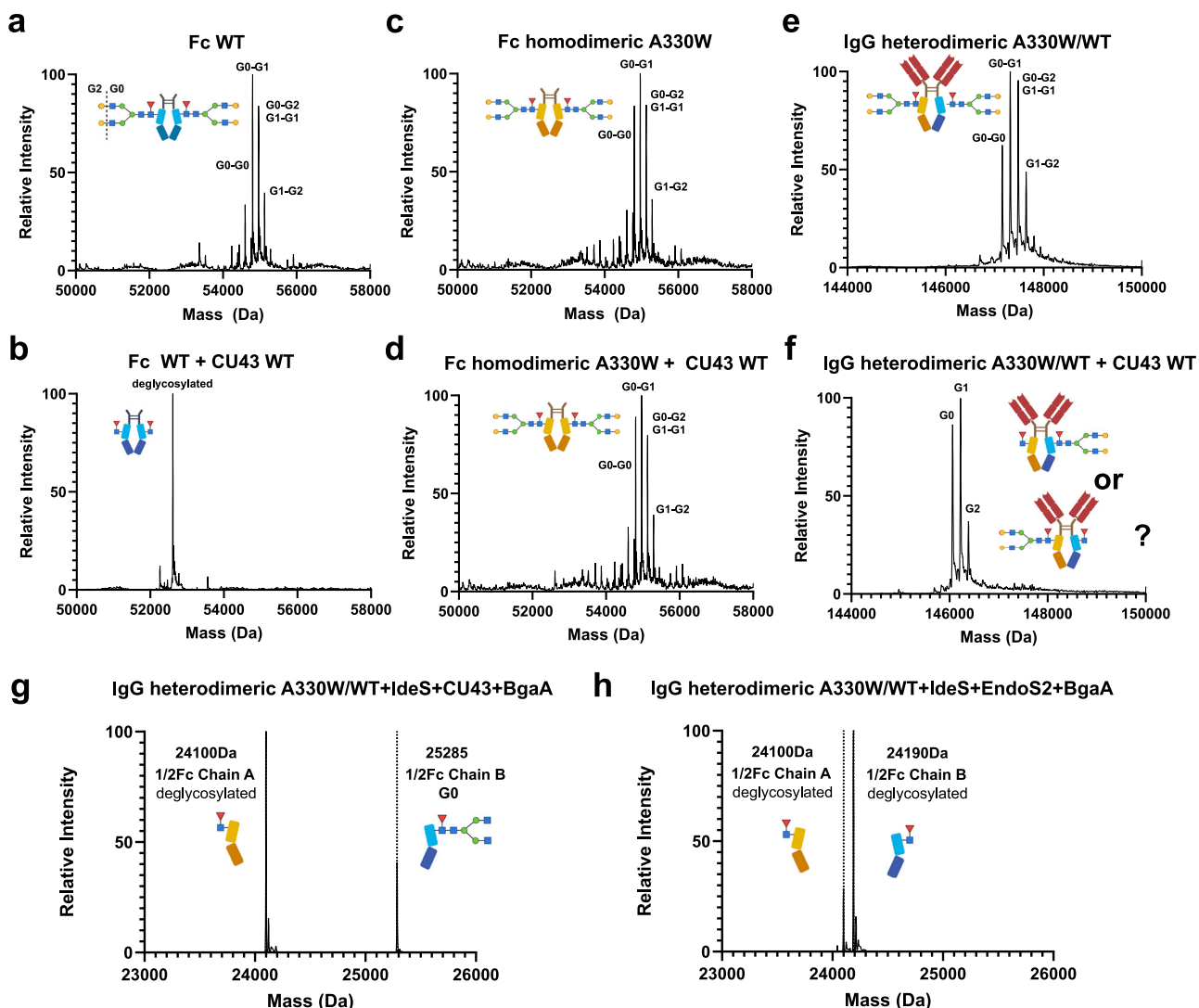


**Fig. 5 | CU43 hydrolyzes IgG glycans by an inter-protomer mechanism.** **a, b** Mass spectrometry analysis of Fc WT CT containing N297- attached CT *N*-glycans incubated with (a) PBS or (b) after treatment with CU43 WT. Glycoforms on Fc are represented as cartoons. **c-d** MS spectra of Fc WT glycoforms from Fc region of IgG1 homodimeric mutant variant harboring a A330W mutation in both protomers (chains A and B), incubated with (c) PBS or (d) after treatment with CU43 WT (1:1,000 enzyme:substrate molar ratio incubated during 3 hs at 37 °C). **e, f** MS spectra of IgG1 heterodimeric variant harboring a mutation A330W only in protomer A (chain A), incubated with (e) PBS or (f) after treatment with CU43 WT (1:1,000 enzyme:substrate molar ratio incubated during 3 h at 37 °C). **g, h** 5 μM IgG1

heterodimeric variant harboring A330W only in protomer A (chain A) after treatment with 50 nM (g) CU43 or (h) EndoS2, and additionally treated with 75 nM IdeS peptidase and 50 nM BgaA (exo-galactosidase), after incubation for 1 h at 37 °C. In panels (E-H) the substrate was IgG Rituximab based KiH heterodimer: Protomer A: T366S/L368A/Y407V/A330W (~5Da); Protomer B: T366W (+ 85 Da). Assays were run in independent duplicates. Blue squares represent GlcNAc, red triangles represent Fucose, Green circles represent Mannose and yellow circles represent Galactose. Schematic Figures were created in BioRender. Sastre, D. (<https://Biorender.com/uh09kf7>). were created in (<https://Biorender.com>). Source data are provided as a Source Data file.

surface between the CH2-CH3 domains and we analyzed the ability of CM49 to deglycosylate this Fc variant. CM49 was unable to remove the *N*-glycans from this Fc triple mutant but was able to fully deglycosylate Fc WT. CU43 showed full activity against both the WT and this Fc mutant, as we evidenced by LC-MS analysis (Supplementary Fig. 11a-f). Additionally, we generated a truncated mutant of CM49 by removing its first 20 residues (CM49 ΔN-term) to evaluate the accuracy of the AF3 model's complex prediction. As anticipated, this mutant variant was entirely incapable of processing *N*-glycans on Fc IgG, despite exhibiting thermostability comparable to the wild-type enzyme (Supplementary Fig. 12a-c). Such a binding mode suggests that CM49, like CU43, also uses an inter-protomer mechanism to deglycosylate IgG antibodies. Despite its unique Fc binding site, CM49 exhibits the hallmarks of CU43 and other IgG-specific ENGases, including 1:1

ENGase:Fc region stoichiometry, as shown by SEC-SAXS (Fig. 7j and Supplementary Table 1), and strict specificity for N297-linked *N*-glycans on native IgG antibodies (Supplementary Fig. 13a-c). Indeed, CM49i was able to interact with IgG1 (CT) at micromolar affinity by SPR analysis in which IgG was immobilized on a Protein A sensor chip, confirming that the specific binding of CM49 to the Fc region is not overlapping with the Protein A binding region (Supplementary Fig. 13d).

## Discussion

We recently discovered a family of single-domain corynebacterial IgG-specific ENGases and showed that the prototypical member of this family, CU43, is required to bind to both the protein and glycan components of the IgG antibody to hydrolyze the *N*-glycans<sup>17</sup>.

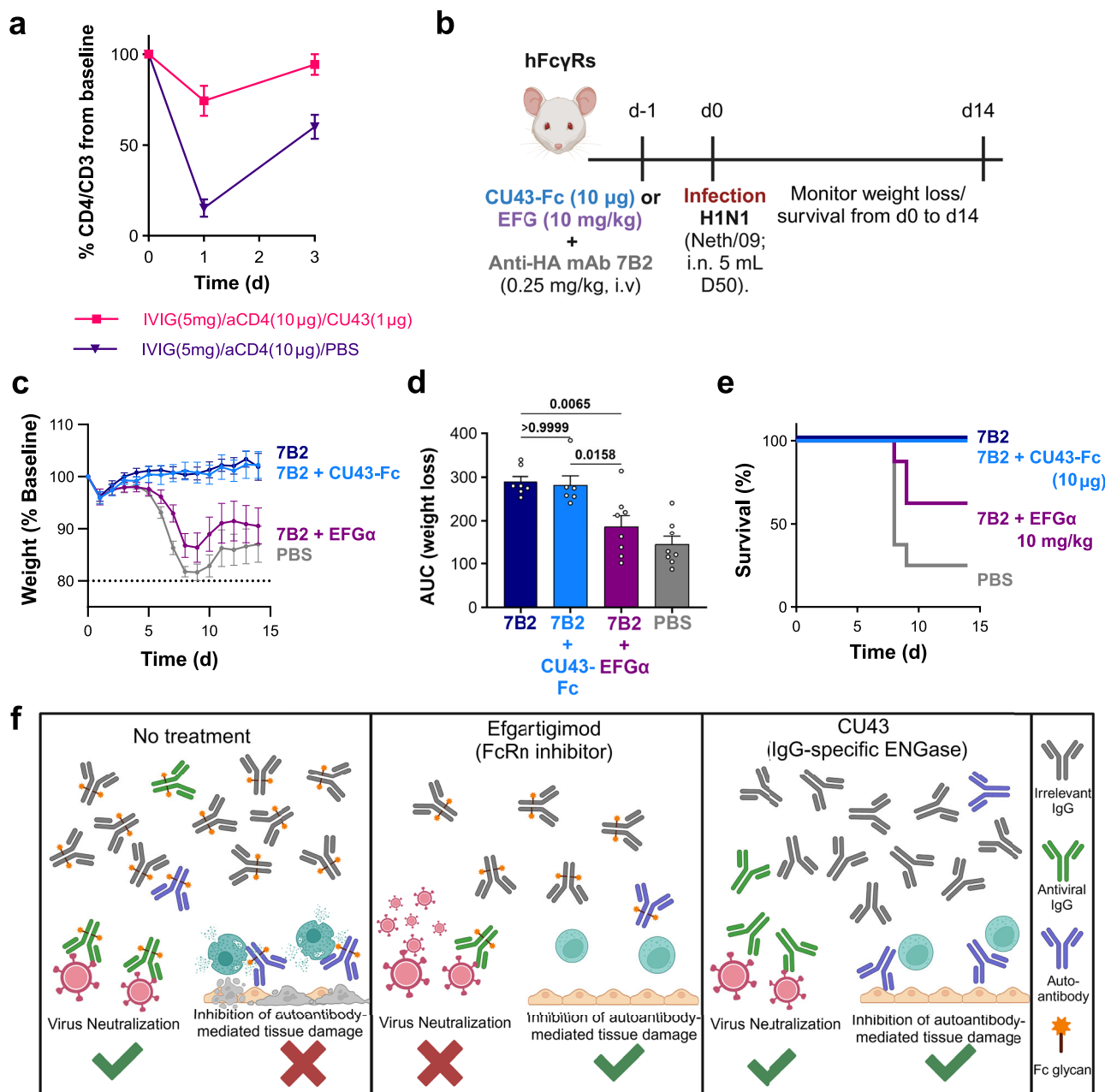
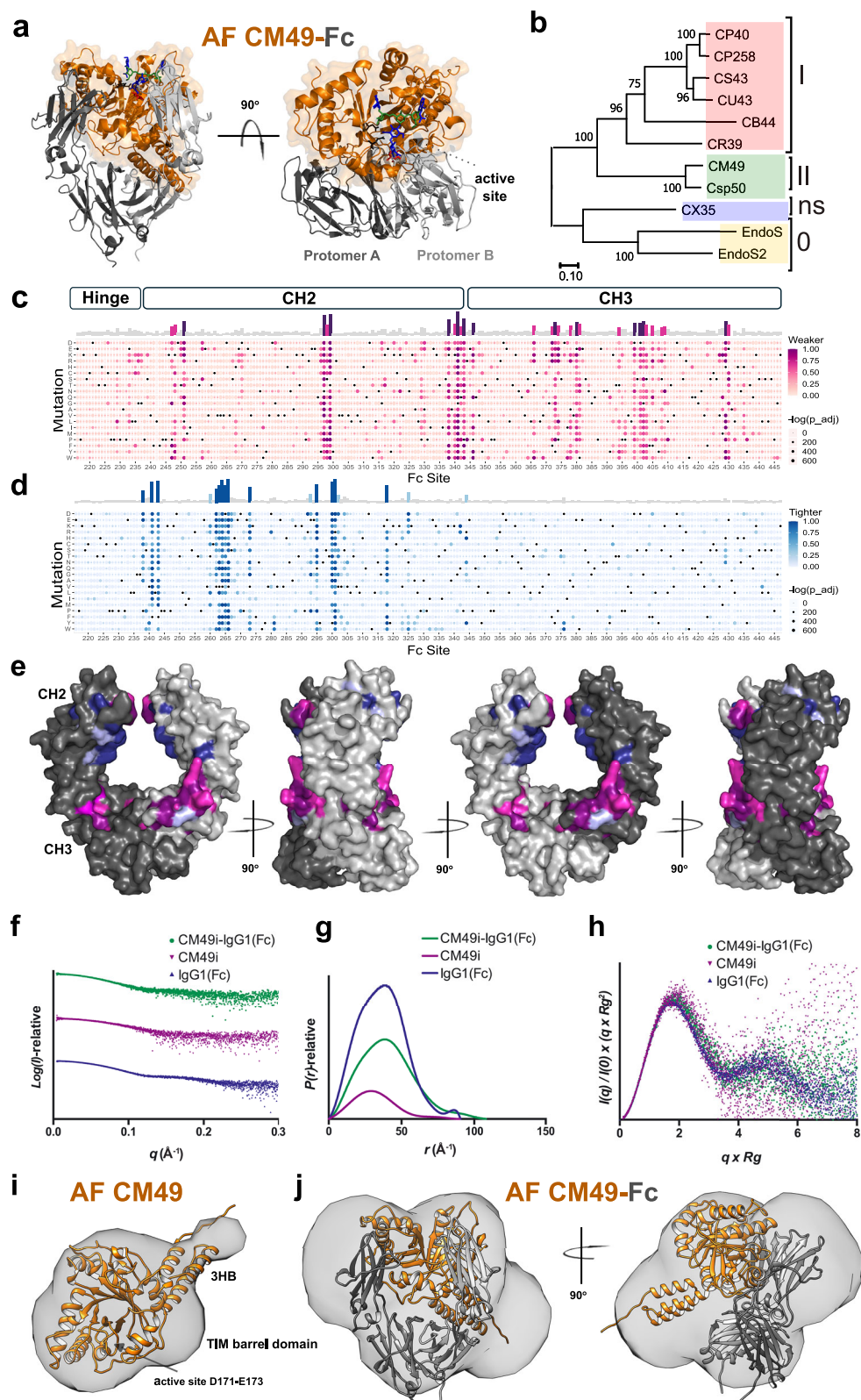


**Fig. 6 | CU43 decouples the effector functions and neutralization capacities of IgG antibodies.** **a** Fc $\gamma$ R humanized mice ( $n=3$ /group) were administered i.v. with the indicated dose of the chimeric rat anti-mouse CD4 mAb (clone YTS191) expressed as afucosylated wild-type (WT) human IgG1. hFc $\gamma$ R mice, 6–8 weeks old. IVIG (IVIG Gammagard (Takeda) NDC 0944-2700-04) 5 mg/mouse (s.c.) + YTS191 afuc (aCD4) 10 $\mu$ g/mouse (i.v.) + CU43 1 $\mu$ g/mouse (i.v.); IVIG 5 mg/mouse (s.c.) + YTS191 afuc (aCD4) 10 $\mu$ g/mouse (i.v.) + PBS (i.v.); The levels of CD4 + T cells in the blood were determined by flow cytometry. Data are presented as mean values  $\pm$  SEM from two independent experiments ( $n=5$  mice/group). **b** Schematic representation of CU43-Fc and Efgartigimod treatment to evaluate the capacity of neutralizing anti-influenza HA mAbs to confer in vivo protection against lethal

influenza challenge in Fc $\gamma$ R humanized mice. **c–e** Fc $\gamma$ R humanized mice ( $n=6$ –8 mice/group) were treated (i.v.) with the indicated dose of CU43-Fc or Efgartigimod (EFG) along with the neutralizing anti-HA mAb 7B2 (0.25 mg/kg, i.v.) one day prior to lethal challenge with H1N1 (Neth/09; i.n. 5mLD50). Weight (**c**, **d**) and survival (**e**) were monitored for a period of 14 days post-infection and compared between groups. AUC=area under the curve. Results are presented as the mean  $\pm$  SEM from two independent experiments ( $n=6$ –8 mice/group). **f** Schematic representation of the effect of IgG degrader vs IgG defector on antibody-mediated functions and neutralization capacities. Schematics in panel 6b and 6f were created in BioRender. *Sastre, D.* (<https://Biorender.com/uh09kf7>) and *Bournazos, S.* (<https://Biorender.com/7f9t1z4>), respectively. Source data are provided as a Source Data file.

Here we describe the molecular mechanism by which CU43 specifically deglycosylates IgG antibodies. We had previously defined the mechanisms by which the multi-domain streptococcal ENGases EndoS and EndoS2 exert strict specificity for the N297-linked glycan on IgG antibodies<sup>10,11</sup>. The multi-domain enzymes follow four molecular rules for IgG-specific deglycosylation: (1) they possess a constrained glycan binding site that prohibits their recognition of non-IgG glycans; (2)

they use a non-enzymatic domain to form a protein-protein interaction with the IgG Fc; (3) their unique multi-domain molecular architecture places the active site in a position to accommodate and hydrolyze the N297-linked glycan upon a conformational rearrangement of the glycan loop; and (4) they deglycosylate IgG sequentially by an intraprotoamer mechanism, binding and hydrolyzing the N297-linked glycan on one Fc protomer prior to binding and hydrolyzing the N297-linked



glycan on the other Fc protomer. Here, we show that CU43 follows these similar rules for IgG specificity with several accommodations for possessing only a single domain. First, on account of CU43 having only one domain, it uses its N-terminal region, which lies distant to the active site to form a protein-protein interaction with IgG, positioning the active site of the enzyme in close proximity to the N297-linked glycan. Second, CU43 deglycosylates IgG by an inter-protomer

mechanism, whereby it binds to one Fc protomer to hydrolyze the N297-linked glycan on the other Fc protomer; like EndoS, CU43 also deglycosylates IgG sequentially<sup>17</sup>.

Having described the mechanism by which CU43 deglycosylates IgG, we then employed a variety of complementary and confirmatory techniques, most notably screening of a site-saturation library of the IgG1 Fc region<sup>18</sup> combined with AF3 modeling<sup>19</sup> to define the molecular

**Fig. 7 | CM49 utilizes a unique binding site on the Fc region to deglycosylate IgG antibodies.** **a** Two views of cartoon representation of AF3 models of CM49 (orange)-Fc dimer (gray) complex. N-glycan GOF was docked into AF-CM49 glycan binding pocket. **b** Neighbor-joining phylogenetic tree of corynebacterial and streptococcal ENGases with bootstrap values (1000 replicates). Protein sequence alignments were performed by MUSCLE and the phylogenetic tree was generated using MEGA v11<sup>47</sup>. O: indicates mechanism of multi-domain IgG-specific ENGases EndoS/S2; I: indicates mechanism of CU43 and its closest homologs; II: indicates the mechanism of CM49 and Csp50; ns, means non-IgG specific ENGase. **c, d** Heatmaps of deep mutational scanning results for IgG1 Fc mutants with **(c)** weaker and **(d)** tighter binding to CM49i. Average tighter/weaker binding scores per site are depicted as bar charts above the heatmaps, with sites highlighted if the score

exceeds one (light blue/pink) or two (dark blue/magenta) standard deviations above the mean. **e** Average tighter (dark/light blue) and weaker (magenta/pink) binding scores, color-coded according to the threshold values described in **(c, d)**, mapped onto Fc dimer structure (PDB code: 5J1H). For statistical analysis of DMS data we used two-sided Fisher's exact test, followed by Bonferroni correction. **e-i** SAXS analysis of the CM49i-IgG1(Fc) complex. **f** SAXS scattering curve of CU49i, IgG1(Fc) and CU49i-IgG1(Fc). **g** P(r) functions distributions of CU49i, IgG1(Fc) and CU49i-IgG1(Fc) complex. **h** Ab initio modeling with GASBOR of the envelope of CM49i and superimposition of CM49i AlphaFold structure prediction. **i, j** Ab initio modeling with GASBOR of the envelope of **(i)** CM49i-Fc and **(j)** superimposition of CM49i-Fc AF3 structure prediction.

mechanisms of IgG specificity for the entire family of corynebacterial IgG-specific ENGases. We describe three distinct mechanisms that partition according to sequence identity. CU43 and its homologs, (CP258, CP40, CS43, CB44, CR39) form a subfamily that uses the mechanism described for CU43 above. CM49 and Csp50 form a subfamily that uses an entirely different binding site on the Fc region to position their active sites proximal to the N297-linked glycan. Finally, CX35 from *C. xerosis*, the most phylogenetically distant ENGase of the family, is a protein-agnostic enzyme, hydrolyzing complex-type glycans from both IgG and non-IgG glycoprotein substrates, as we had shown previously<sup>17</sup>.

The IgG Fc region has two distinct hotspots for binding by host receptors, as well as pathogenic proteins and enzymes (Fig. 8). The top surfaces of the two CH2 domains, one from each protomer, form a binding site for FcγRs<sup>26</sup> and complement C1q<sup>27</sup>– host receptors that control antibody-mediated effector functions – as well as for IdeS and, now, CU43 sub-family ENGases – pathogenic IgG-specific enzymes that defeat antibody-mediated effector functions via degradation or deglycosylation, respectively. This binding site is asymmetric in that the amino acid residues forming the binding interface on one Fc protomer are distinct from those on the other Fc protomer. The other prominent binding site on the Fc region is formed by the outer surface of the intersection of the CH2 and CH3 domains. This site is targeted by FcRn, which is responsible for IgG recycling and the long serum half-life of these antibodies, Protein A and Protein G, bacterial proteins that disrupt opsonization and phagocytosis, as well as EndoS and EndoS2, the multi-domain streptococcal IgG-specific ENGases. This site is symmetrical in that binding to one Fc protomer allows for identical binding to the other Fc protomer. Members of the CM49 sub-family of single-domain IgG-specific ENGases bind an entirely unique site formed by the inner surface of the intersection of the CH2 and CH3 domains that does not overlap with either of the two above-described hotspots for Fc binding. This expands the catalog of viable recognition sites on the Fc region.

IgG antibodies exhibit two distinct immunological functions – neutralization of microbes and toxins, which is mediated by Fab domain recognition, and antibody-mediated effector functions, which are dependent on Fc region binding to FcγRs and complement C1q. A fully competent immune system requires both functionalities. In the treatment of IgG-mediated pathologies, IgG degraders, either enzymes that degrade IgG directly (e.g., IdeS) or proteins that block FcRn-mediated recycling to shunt IgG antibodies to proteasomal degradation (e.g., Efgartigimod), nullify both of these properties of IgG antibodies. This form of pharmacologically-induced plasmapheresis cannot abrogate one IgG function without negating the other. Here, we found that CU43, representative of a class of effective in vivo IgG defeaters as well as EndoS<sup>28–30</sup>, which strictly defeat the antibody-mediated effector functions of IgG, fully preserved the neutralization capacity of IgG antibodies in a humanized mouse model of lethal influenza infection, thereby separating the two immunological

properties of IgG antibodies. This selective activity of IgG defeaters may be clinically advantageous.

## Methods

### Expression and purification of bacterial and mammalian proteins

Corynebacterial ENGases CU43 and CM49 ORFs cloned into the pET28a vector between *Bam*H-*Xba*I sites, containing His6 tag on the N-terminus<sup>17</sup>. *Escherichia coli* BL21(DE3) cells (NEB) transformed with the corresponding plasmid were grown in 50–2000 ml of LB medium supplemented with 50 µg ml<sup>-1</sup> kanamycin at 37 °C. When the culture reached an OD<sub>600</sub> value of 0.6–0.8, the expression of proteins was induced by adding 0.25 mM IPTG. After ca. 16 h at 18 °C, the cells were harvested by centrifugation at 6000 × g for 20 min at 4 °C and resuspended in 10–50 ml of 20 mM HEPES, pH 7.4, 300 mM NaCl. Cells were disrupted by sonication (12 cycles of 10 s pulses with 60 s cooling intervals between the pulses, and 60% of amplitude) at 4 °C, and the suspension was centrifuged at 10,000 × g for 10 min at 4 °C. The supernatant was passed through 0.2 µm filters and applied to a NiNTA column (1–5 ml, Thermo Scientific) equilibrated with 20 mM HEPES, pH 7.5, 300 mM NaCl. The elution was performed with a linear gradient of 0 to 500 mM imidazole in 20 ml of solution A at 1 ml/min. The eluted fractions were buffer exchanged to 20 mM HEPES pH 7.4, 150 mM NaCl, pH 7.4 in an Amicon Ultra-15 centrifugal filter unit (Millipore) with a molecular weight cutoff of 10 kDa at 4000 × g. Proteins were further purified by size-exclusion chromatography using a Superdex 200 10/300 GL column (GE Healthcare) equilibrated in 20 mM HEPES pH 7.4, 150 mM NaCl, pH 7.4. The eluted protein was concentrated using an Amicon Ultra-15 centrifugal filter unit (Millipore) with a molecular weight cutoff of 10 kDa at 4000 × g. Samples from the purification steps were analyzed by SDS-PAGE.

The primers for alanine scanning mutagenesis were designed using the NEBaseChanger website (<https://nebasechanger.neb.com/>) and purchased from IDT (Integrated DNA Technologies, Inc, Iowa, USA) and PCR was carried out using the NEB Q5 Site-Directed Mutagenesis Kit and the manufacturer's instructions. List of primers sequences used in this study are included in Supplementary Table 3.

Plasmids containing the CU43a-i-Fc, hIgG1-Fc fragment and Efgartigimod alfa (hIgG1-(M252Y/S254T/T256E/H433K/N434F)-Fc fragment<sup>17</sup>) were transfected in Expi293F™ cells (Catalog number: A14527, Thermo Fisher) according to the manufacturers protocol (Catalog: MAN0007814, Thermo Fisher) with the addition of Penicillin/Streptomycin mix 24 h post transfection. The cells were cultured for 96 h before harvesting. The constructs were then purified using Protein A resin (Thermo Fisher) with PBS pH 7.4 being used as the binding buffer and 100 mM sodium citrate buffer pH 3.0 as the elution buffer. The fractions were neutralized with 1 M Tris pH 9.0. The proteins were buffer exchanged into 1x PBS using a 50 kDa Amicon Ultra Centrifugal Filter (Millipore).

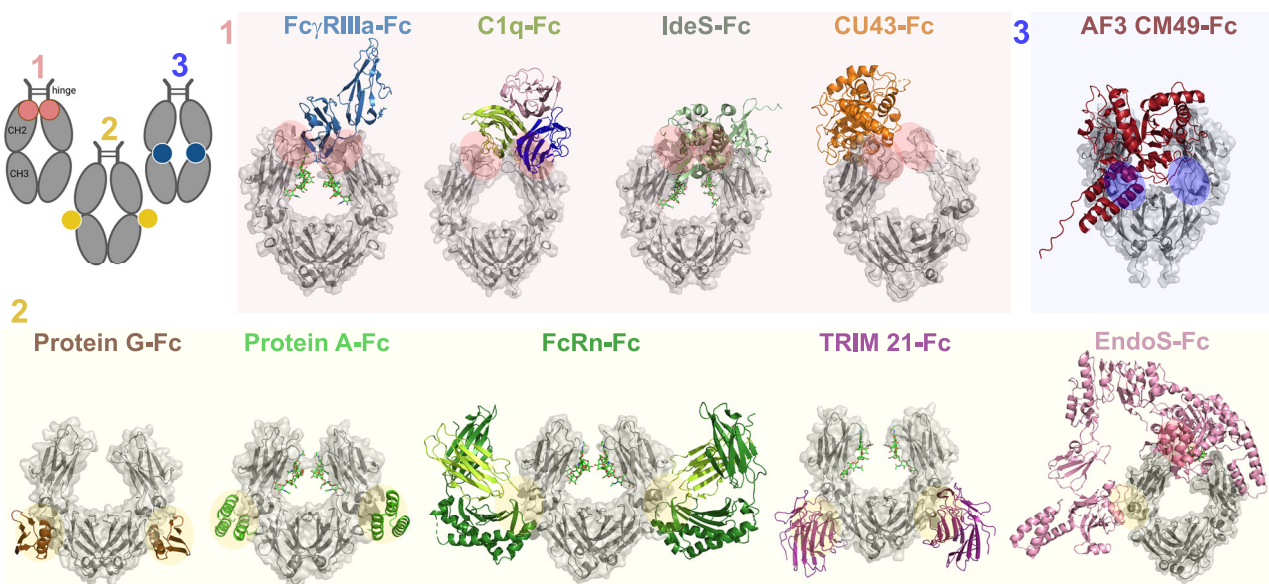


**Fig. 8 | CM49 binds a unique site on Fc IgG1 that does not overlap with any described hotspots for Fc binding.** Structural comparison of diversity of binding sites of proteins that specifically interact with IgG1 Fc. (1) top of CH2 binding: FcγRIIIa-Fc (PDB code: 1E4K), C1q-Fc (PDB code: 6FCZ), IdeS-Fc (PDB code: 8A47) and CU43i-Fc (PDB code: 8EURO); (2) external surface of CH2-CH3 elbow: ProteinA-

Fc (PDB code: 5U4Y), Protein G-Fc (PDB code: 1FCC), FcRn-Fc (PDB code: 7Q15), TRIM 21-Fc (PDB code: 2IWG) and EndoS-Fc (PDB code: 8A64); (3) CM49 bind to the inside surface of the CH2-CH3 elbow while no other Fc-binding protein or enzyme is known to bind to this site. Schematics were created in BioRender. Sastre, D. (<https://BioRender.com/uh09kf7>).

### Antibody purification

After transfection, cells were cultured for 96 h in Free-style F17 medium supplemented with GlutaMAX and Geneticin (Thermo Fisher Scientific). IgG1 was purified using protein A chromatography, with 20 mM sodium phosphate buffer pH 7.0 used as a binding buffer and 100 mM sodium citrate buffer pH 3.0 as elution buffer. The fractions were neutralized with 1 M Tris pH 9.0. SDS-PAGE was used to identify fractions which contained IgG1. These were subsequently pooled, concentrated and analyzed by LC-MS. Heterodimeric IgGs were obtained from co-expression of the following heterodimeric platform and the mutations on one heavy chain are based on the knobs-into-holes (KiH) strategy<sup>31</sup> in which Protomer A contains mutations T366S/L368A/Y407V/A330W (~5Da) and Protomer B only mutation T366W (+ 85 Da). List of protein constructs expressed is included in Supplementary Table 4.

### Crystallization and data collection

CU43i-Fc was crystallized by mixing 0.9 μL of a protein solution at 10 mg mL<sup>-1</sup> in 20 mM Buffer HBS pH 7.4, 150 mM NaCl with 0.6 μL of MIDAS (2-31) solution (0.2 M ammonium acetate 0.1 M MES 6.5 30 %v/v glycerol ethoxylate) and 0.3 μL of seed stock from crystal of the complex obtained in (PACT 2-17). Crystals were transferred into a solution of cryo-protectant solution containing 20% glycerol and frozen under liquid nitrogen. Complete X-ray diffraction datasets were collected at the Southeast Regional Collaborative Access Team (SER-CAT) Beamline 22-ID facilities at the Advanced Photon Source (APS) at the Argonne National Laboratory, IL (USA). The wavelength of data collected was 1.0. CU43i-Fc crystallized in space groups P2<sub>1</sub> with two molecules in the asymmetric unit (with ~65% solvent content) and diffracted to a maximum resolution of 3.6 Å (PDB code 8EURO) (Supplementary Table 2). Datasets were integrated and scaled with HKL2000 following standard procedures.

### Structure determination and refinement

The structure determination of the CU43i-Fc<sup>E382S</sup> complex was solved by molecular replacement methods implemented in Phaser and the PHENIX suite using the crystal structure of CU43i (PDB code: 8UEN)

and Fc (PDB code: 5J1H) as search models. Owing to the large structural reorganization of the molecules upon complex formation, Phaser yielded a single solution in space group P12<sub>1</sub>1 for the positioned Fc fragment. With the positioned Fc part, the ENGase CU43 was found with a clear solution (LLG = 1286 TFZ = 32.8). Structure refinement was performed using Coot and phenix.refine. The positioned molecules fitted into the asymmetric unit without sterical clash. By refinement considering each domain as a rigid unit the analysis was extended stepwise to the resolution of 3.6 Å and the large relative movements of the individual domains became apparent. An overall B-factor refinement resulted in high B-factors with a large anisotropic contribution, in accordance with the prediction from the Wilson plot. This might be an intrinsic property of the Fc fragment, which has also been observed in other complex structures where parts of the Fc fragment were found disordered<sup>26</sup>. The calculated electron density at 3.6 Å was of sufficient quality to trace the backbone of the polypeptide chains, however, some ambiguities in the main chain peptide orientations remained. Most CH2 backbone in chain B (Protomer B) were not visible in the electron density. For Figs. 3 and 4, protomer B on CU43i-Fc<sup>E382S</sup> structure was replaced with a copy of Fc from PDB (code: 5J1H) to show all mutated residues. Ramachandran statistics indicated that 94.15 (%) of protein residues were in favored regions, 3.66 % of residues were in allowed regions and 2.18% were in disallowed regions. The structures were validated by MolProbity. Data collection and refinement statistics are presented in Supplementary Table 2. Molecular graphics and structural analyses were performed with Pymol (PyMOL Molecular Graphics System, Version 1.2r3pre, Schrödinger, LLC) and UCSF Chimera v1.6. Protein-glycan docking analysis of CU43 and N- glycan (GlcNAc(b1-2)Man(a1-3)[GlcNAc(b1-2)Man(a1-6)]Man(b1-4)GlcNAc(b1-4)[Fuc(a1-6)]GlcNAc, also called GOF) was performed using default settings on HADDOCK 2.4 server<sup>32</sup>. We used the online server US-align (Version 20241108, <https://zhanggroup.org/US-align/>) to calculate TM-score of protein complexes<sup>33</sup>.

### IgG1 Fc cell line generation for mammalian surface display

The IgG1 Fc cell line generation and mammalian surface display platform were as described in ref. 18. Our construct consisted of codon-optimized

IgG1 Fc (UniProt ID: P01857, residues 216-447) preceded by an N-terminal signal peptide sequence derived from IgG4 (MEFGLSWVFL-VALFRGVQC), 1xGGS linker, Myc-tag (EQKLISEEDL) and 2xGGS linker, and followed by a transmembrane helix derived from PDGFR (AVGQDTQEIVVPHSLPFKVVVISAILALVLTISLIIILWQKKPR). We cloned this sequence into pLVX-IRES-ZsGreen1 (TakaraBio) at the EcoRI and NotI sites using Gibson assembly (NEB 2x Gibson Assembly Master Mix) and packaged the resulting construct into a lentivirus using the vectors psPAX2 and pMD2G and the LV-MAX lentiviral production system (ThermoFisher) in a 1:1:0.5 pLVX:psPAX2:pMD2G ratio. A stable cell line of lentivirus-infected Viral Production Cells was then generated at a multiplicity of infection of 0.1, resulting in >90% of cells being infected with a single viral particle.

### Site-saturation library generation

Site-saturation library generation was as described in ref. 18. Briefly, a site-saturation library containing every possible mutation at positions 216-447 of the IgG1 protein sequence (UniProt ID: P01857) was synthesized (TwistBioscience). 15-nucleotide barcodes were added by PCR using 5 amplification cycles with pLVX\_IgG4\_FW and pLVX\_BC\_PDGFR\_RF primers. The resulting DNA was packaged into pLVX-IRES-ZsGreen at the EcoRI and NotI sites using Gibson assembly (NEB). The reaction mixture was electroporated using Endura<sup>TM</sup> Electrocompetent Cells (Lucigen) and plated on LB ampicillin plates to concentrations set to achieve ~150,000 colonies per replicate library (to limit library complexity), and grown overnight at 30 °C. The following day, the cells were washed from the plates, and the plasmids were purified using a HiSpeed Plasmid Maxi kit (Qiagen). These replicate libraries were then packaged into a lentiviral library as described in the previous section. Titration of these lentivirus preparations using the GFP reporter was then performed, where 200 million Viral Production Cells were infected at an MOI of 0.1 to generate stable cell lines. 48 h post-transfection, cells were harvested and filtered with 0.45 µM, 25 mm PES filters. A FACS ARIA II instrument (BD), administered by the Emory Flow Cytometry Core, was then used to collect at least 5 million GFP-positive cells. These GFP-positive cells were then expanded and stained with a rabbit Alexa647-anti-Myc antibody (Cell Signaling, 1:200 dilution), before sorting for cells expressing functional Fc mutants. A minimum of 5 million GFP<sup>+</sup>/Myc<sup>+</sup> cells were sorted and expanded for each replicate library, to be used for screening against the endoglycosidases.

### Flow cytometry to characterize IgG1 Fc WT binding

Binding studies for IgG1 Fc WT with CU43i, CM49i and EndoS2 was as described for Fc with Fc gamma receptors from<sup>18</sup>. Briefly, binding to each endoglycosidase was individually measured using our cell line stably expressing wild-type IgG1 Fc on the cell surface. Biotinylated endoglycosidases were prepared in binding buffer and incubated with ~5 × 10<sup>4</sup> cells for 1 h at room temperature. Cells were then washed four times with binding buffer and stained with rabbit PE-labeled anti-Myc antibody and PerCP-eFluor<sup>TM</sup> 710-labeled streptavidin (ThermoFisher). Data collection was conducted using a Northern Lights (Cytek) instrument, and the median fluorescence intensity (MFI) of PerCP-eFluor710 used to measure the binding between Fc-expressing GFP<sup>+</sup>/Myc<sup>+</sup> cells and the biotinylated endoglycosidases.

### PacBio library sequencing and analysis

The library used in this study was the same as that used in ref. 18. For details, see that report and our GitHub page ([https://github.com/Ortlund-Laboratory/DMS\\_IgG1Fc/tree/main](https://github.com/Ortlund-Laboratory/DMS_IgG1Fc/tree/main)).

**Fluorescence-activated cell sorting of library to select mutants that cause tighter/weaker binding to CU43i, CM49i and EndoS2**  
Fluorescence-activated cell sorting (FACS) with this library was as described for assays with Fc gamma receptors in ref. 18. Briefly, for

each assay, 30 million GFP<sup>+</sup>/Myc<sup>+</sup> IgG1 Fc library cells were washed with binding buffer (1X PBS plus 2% FBS and 10 mM HEPES, pH 7.5) and incubated with CU43i/CM49i/EndoS2 at concentrations approximating the  $K_D$  of the relevant Fc-enzyme interaction in a combined volume of 0.5 mL at room temperature for 1 h. Following a further three washes with additional binding buffer, the cells were stained with rabbit anti-Myc antibody and PerCP-eFluor<sup>TM</sup> 710 streptavidin. A BD FACSMelody<sup>TM</sup> cell sorter (BD Biosciences) or a BD FACS Aria II instrument (BD Biosciences) was used for cell sorting. Positive anti-Myc signal was used as a control for cell surface expression, and so cells were selected above the diagonal to capture the top 15% of binders (the tightest-binding mutations) and below the diagonal to capture the bottom 15% of binders (the weakest-binding mutations) on an anti-Myc vs enzyme signal plot. ~1 × 10<sup>6</sup> cells were collected in LV-MAX production medium for both the tighter- and weaker-binding populations. Additionally, an unsorted reference population (5 × 10<sup>6</sup> cells) was collected per experiment. FACS experiments were carried out in the Flow Cytometry Core Facility of the Emory University School of Medicine.

### High-throughput sequencing

Preparation of cells for sequencing was as described in ref. 18. Briefly, cells were washed once with 1X PBS, the RNA extracted using a GenJet RNA Purification Kit (ThermoFisher) and cDNA prepared using a High-Capacity cDNA Reverse Transcription Kit (ThermoFisher) and with a primer designed to anneal immediately downstream of the barcode sequence. Barcodes were then amplified over 8 rounds of PCR (increasing to 15 if necessary) using a Platinum<sup>TM</sup> SuperFi<sup>TM</sup> DNA polymerase (ThermoFisher). Samples were sequenced on an Illumina NovaSeq 6000 at PE100 or PE26x91, with a read-depth of 10 million reads for a tighter- or weaker-binding population, and a read-depth of 50 million reads per reference sample. Next generation sequencing services were provided by the Emory NRPC Genomics Core.

### Calculation of binding scores for sequencing data analysis

The calculation of tighter- and weaker-binding scores was as described in ref. 18. Notebooks were adapted from those developed by the Bloom group (see the dms\_variants package at [https://jbloomlab.github.io/dms\\_variants/index.html](https://jbloomlab.github.io/dms_variants/index.html) and Greaney et al.<sup>34</sup>). Our workflow is given on our GitHub page at [https://github.com/Ortlund-Laboratory/DMS\\_EndoS2 CU43\\_CM49](https://github.com/Ortlund-Laboratory/DMS_EndoS2 CU43_CM49)).

### Data visualization

Custom scripts required for heatmap generation are provided at [https://github.com/Ortlund-Laboratory/DMS\\_EndoS2 CU43\\_CM49/tree/main/Example\\_Workflow/scores\\_and\\_visualization](https://github.com/Ortlund-Laboratory/DMS_EndoS2 CU43_CM49/tree/main/Example_Workflow/scores_and_visualization). The x-axis of each heatmap denotes the site number of IgG1 (ranging from 216-447), and the y-axis denotes the possible amino acid types. Black dots represent the WT sequence, with the other dots color-coded according to binding strength, with an increased hue denoting a stronger score. Bar charts which depict an average of the binding scores per site can also be produced.

### Analytic ultracentrifugation analysis

Sedimentation velocity analytical ultracentrifugation was conducted using an An-50 Ti analytical rotor at 50,000 rpm (182,000 × g) at a nominal temperature of 20 °C in a Beckman Colter XLI analytical ultracentrifuge using standard procedures<sup>35</sup>. CU43i was incubated with Fc CT mixture at a nominal ratio of 2:1 (15 µM CU43i- 7.5 µM Fc dimer) and SEC-purified CU43i and FcCT were run individually. The partial specific volumes of each protein were calculated based on amino acid composition using SEDFIT version 16.36 (<https://spsrch.cit.nih.gov/>). Samples (0.4 mL) were loaded into 12 mm pathlength Epon double sector cells equipped with sapphire windows with matched buffer (20 mM HEPES 150 mM NaCl, pH 7.4) in the reference sector. The buffer density and viscosity at 20 °C were measured using an Anton

Parr DM4500 densitometer and Lovis 2000M viscometer. Absorbance scans at 280 nm were initiated after reaching the target rotor speed and collected at 4.7 min intervals. Data were corrected for scan time errors using REDATE version 1.01<sup>36</sup>. Data were analyzed using the continuous  $c(s)$  distribution model<sup>37</sup> in SEDFIT and a sedimentation coefficient interval of 0 to 10 S at 0.1 S intervals. Data were fitted using sequential simplex and Marquardt-Levenberg algorithms and maximum entropy regularization with a confidence interval of 0.68. The fitted parameters were  $c(s)$ , the frictional ratio ( $f/f_0$ ), time-invariant noise and the meniscus position. Sedimentation coefficients were adjusted to the standard condition of 20 °C in solvent water. Molecular weight estimates were obtained for the dominant species from the Svedberg equation by deconvoluting the contribution of diffusion to the observed signal as described<sup>37</sup>.

### Mass Photometry analysis

CU43i, Fc IgG1 and 1:1 CU43i-Fc complex samples in Buffer PBS containing an additional of 0; 0.5 or 2 M NaCl, were diluted to a final concentration of 50-100 nM (1 μl of 1-2 μM protein in 20 μl final volume) and loaded onto a Refeyn Two<sup>MP</sup> mass photometer. Data was acquired for 60 sec using Acquire MP software. Data analysis was performed using Discover MP software to determine the molecular weight distribution of the protein samples. Calibration was performed using BSA.

### SEC-MALS analysis of the CU43i-Fc complex

The SEC MALS configuration consisted of an isocratic pump/vial sampler/variable wavelength 1 cm pathlength detector (1260 Infinity II HPLC system, Agilent Corporation) in line with a Superdex 200 10/300 GL SEC column (GE Healthcare Life Sciences), DAWN multi-angle light scattering detector and Optilab differential refractometer (Wyatt Corporation). A 0.1 mL mixture of 3.2 mg/mL of CU43i and 1.92 mg/mL of Fc-CT was applied to the SEC column at 0.5 mL/min at room temperature. HPLC control, data acquisition and analysis were performed using ASTRA (version 8.1.2.1) and HPLC Connect (version 2.0; Wyatt Corporation). DAWN measurements of scattering of vertically polarized 658.3 nm GeAs laser light were made at 13 angles ranging from 34 to 134 degrees. Voltage signals from 0.5 s “slices” of the chromatogram were converted to Rayleigh ratios,  $R_\theta$ , by calibrating 90-degree light scattering with toluene according to instructions provided by the manufacturer. Normalization of the scattering at the other angles to the signal at 90 degrees was done using bovine serum albumin as an isotropic scatterer. Normalization, peak alignment and correction for band broadening were performed using ASTRA. Estimates of weight average molecular weight,  $M_w$  were made in ASTRA using the Berry model.

### SEC-SAXS experiments

A 50 μM solution of CU43i or CM49i were incubated with 125 μM solution of Fc-Rituximab (IgG1(Fc)) in 50 mM Tris-HCl pH 7.5, 100 mM NaCl, 2% v/v glycerol for 10 min at room temperature to form the CU43i-IgG1(Fc) or CM49i-IgG1(Fc) complexes. Small-Angle X-ray Scattering coupled with Size Exclusion Chromatography (SEC-SAXS) data for purified CU43i, CM49i, IgG1(Fc) and the complex mixtures of CU43i-IgG1(Fc) and CM49i-IgG1(Fc) in 50 mM Tris-HCl pH 7.5, 100 mM NaCl, 2% v/v glycerol were collected on the B21 beamline of the Diamond Light Source, UK. 50 μL of the protein samples or the complex mixtures were injected into a Shodex KW403-4F column and eluted at a flow rate of 160 μL min<sup>-1</sup>. Data were collected using an EigerX 4 M detector (Dectris, CH) at a sample-detector distance of 3,720.9 mm and a wavelength of  $\lambda = 0.9464 \text{ \AA}$ . The range of momentum transfer of  $0.045 < s < 3.4 \text{ nm}^{-1}$  was covered ( $s = 4\pi s \sin\theta/\lambda$ , where  $\theta$  is the scattering angle). Data were processed and merged using standard procedures by the program package ScAtter<sup>38</sup> and PRIMUS<sup>39</sup>. The maximum dimensions ( $D_{max}$ ), the interatomic distance distribution functions ( $P(r)$ ), and the radii of gyration ( $R_g$ ) were computed using

**GNOM.** The ab initio multiphase reconstruction of the SAXS data of the CU43i-IgG1(Fc)-and the CM49i-IgG1(Fc) complexes were generated using the GASBOR<sup>40</sup> algorithm from ATSAS<sup>41</sup>. The results and statistics are summarized in Supplementary Table 1.

### Hydrolytic activity assays

For enzymatic endpoint assays, we incubated each enzyme with IgG1-Fc region (complex type glycan, IgG substrate) or full-length IgG (Rituximab; complex type glycan). We used all enzymes at final concentrations of either 5–50 nM and the reactions were run at 37 °C in final volume of 20 μL containing 5 μM of the Fc in PBS pH 7.4, before analyzing the progress of the enzymatic reactions by intact mass spectrometry. The reactions were analyzed by LC-MS using an Agilent 1290 Infinity II LC System equipped with a 50 mm PLRP-S column from Agilent with 1000 Å pore size attached to an Agilent 6545XT quadrupole-time of flight (Q-TOF) (Agilent, Santa Clara, CA). The reactions were set up and placed in the LC-MS and the reactions were sampled approximately every 6.5 min until they reached completion. All reactions were performed in triplicate. Relative amounts of the substrate and hydrolysis products were quantified after deconvolution of the raw data and identification of the corresponding peaks using BioConfirm10.0 (Agilent, Santa Clara, CA) as described in ref. 42.

To obtain the rate of deglycosylation on targeted mutagenesis assays, the relative proportions of the diglycosylated, monoglycosylated and deglycosylated products were imported into Kintek Global Kinetic Explorer<sup>43</sup> as described in ref. 42. All replicates for an experiment were fitted globally within the software.

### Surface plasmon resonance (SPR)

SPR experiments were performed by using a Biacore X100 instrument (GE Healthcare) from the Glycomics Core at Emory University. For SPR experiments, we used a protein A sensor chip (GE Healthcare). Concentration series of CM49i were injected and affinity constants were calculated. Concentration series of proteins (μM range), in HBS-EP running buffer (10 mM HEPES, 150 mM NaCl, 0.005% Tween 20, EDTA 3 mM) were injected over flow cells 1 and 2 for 120 s per injection and allowed to dissociate for 600 s. Injection of IgG CT (diglycosylated), IgG aglycosylated (N297A) on Flow cell2 (up to 400 RU, 15 nM of IgG1) and then injection of serial dilutions of inactive enzyme as analyte. Protein A chip regeneration was performed by one step of 20 mM HCl in each cycle. Affinity constants for CM49i were calculated using a general steady-state equilibrium model in the Biacore X100 evaluation software.

### Protein thermal stability

The thermal stability of CM49 WT and mutant variant was evaluated using nano differential scanning fluorometry (nanoDSF) method in PBS buffer using 5–10 μM final concentration of enzyme. The sample was loaded into standard treated capillaries and measured in the Prometheus NT.48 instrument (NanoTemper, Munich, Germany). Absorbance at 350/330 nm of the sample was recorded for each 1 °C increment of temperature in the range 25–90 °C. The first derivative of the melting curves was analyzed in GraphPad Prism v.10.4 software and the  $T_m$  of each protein in each condition were calculated.

### Quantification of serum levels of CU43-Fc levels

Blood from mice was collected into gel microvette tubes, serum was fractionated by centrifugation (10,000  $\times g$ , 5 min) and stored at -20 °C. The serum levels of CU43-Fc were determined by ELISA. Briefly, high-binding 96-well microtiter plates (Nunc) were coated overnight at 4 °C with Neutravidin (ThermoFisher, 2 μg ml<sup>-1</sup> in PBS). All subsequent steps were performed at room temperature. Plates were blocked for 2 h with PBS/2% (w/v) bovine serum albumin and incubated with biotinylated goat anti-human IgG antibodies for 1 h (Jackson Immunoresearch; 5 μg ml<sup>-1</sup>). Serum samples were serially diluted and incubated for 1 h,

followed by incubation with horseradish peroxidase-conjugated anti-human IgG (1:5,000; Jackson ImmunoResearch, Cat# 109-035-008). Plates were developed using the 3,3',5,5'-tetramethylbenzidine (TMB) two-component peroxidase substrate kit (KPL), and reactions were stopped with the addition of 1M phosphoric acid. Absorbance at 450 nm was immediately recorded using a SpectraMax Plus spectrophotometer (Molecular Devices), and background absorbance from negative control samples was subtracted.

## Cells and viruses

Experiments were performed using a derivative of the HEK 293 F cell line called “Viral Production Cells” from the ThermoFisher LV-MAX Lentiviral Production system (Cat. No. A35684). Cells were cultured in LV-MAX Production medium due to its ability to grow cells up to high densities (up to  $10^7$  cells/mL). The A/Netherlands/602/09 (Neth09) H1N1 virus was grown in 10-d-old specific-pathogen-free embryonated chicken eggs (Charles River Laboratories, Wilmington, MA) as previously described<sup>44</sup>.

## Animals

In vivo experiments were approved by the Rockefeller University Institutional Animal Care and Use Committee in compliance with federal laws and institutional guidelines. IACUC Protocol Number 23018-H. Experiments were conducted using both male and female mice maintained in the Comparative Bioscience Center at Rockefeller University with a 12 h day:night cycle at a controlled ambient temperature (20–25 °C) and humidity (30–70%). All injections were retro-orbital. FcγR humanized (mFcγR $\alpha^{-/-}$ , FcgrI $^{-/-}$ , hFcγRI $^{+/-}$ , hFcγRIIa $_{R131}^{+/-}$ , hFcγRIIb $^{+/-}$ , hFcγRIIa $_{F158}^{+/-}$  and hFcγRIIb $^{+/-}$ )<sup>45</sup> mice were previously developed and fully characterized.

## CD4 + T cell depletion

FcγR humanized mice were anesthetized (isoflurane (3%) in a VetFlo high-flow vaporizer) and co-injected with the indicated dose of CU43-Fc, CU43-Fc variants, or PBS followed by YTS191-Afucosylated (10 µg). Peripheral blood was collected one day pre-injection and one- and three-days post-injection. Blood was lysed (RBC lysis buffer; Biolegend), resuspended in PBS containing 2% (w/v) BSA and 5 mM EDTA, and analyzed by flow cytometry using the following mixture of fluorescent antibodies (all used at 1:250 dilution): anti-mouse CD8a (clone 53-6.7)-FITC (BioLegend, Cat# 100737), anti-mouse CD45 (clone 30-F11)-PE/Cy7 (BioLegend, Cat# 103140), anti-mouse CD11b (clone MI/70)-Brilliant Violet 711 (BioLegend, Cat# 101215), anti-mouse CD4 (clone RM4-4)-PE (BioLegend, Cat# 116005), anti-mouse CD3e (clone 145-2C11)-PerCP/Cy5.5 (BioLegend, Cat # 100327). Flow cytometry data were collected using an Attune NxT flow cytometer (ThermoFisher) with Attune NxT software v.3.1.2 and analyzed using FlowJo (v.10.10) software.

## Lethal influenza virus challenge assay

Lethal challenge of FcγR humanized mice with influenza virus was performed as described previously<sup>46</sup>. Briefly, mice (males or females; 10–18 weeks old) were anesthetized with a ketamine (75 mg kg $^{-1}$ ) and xylazine (15 mg kg $^{-1}$ ) mixture (administered i.p.) and challenged intranasally (30 µl) with 5 mL $_{50}$  A/Netherlands/602/09 (Neth09) H1N1 (diluted in PBS). After the infection, mice were monitored daily, and their weights were recorded for 14 days. Death was determined by a 20% body weight loss threshold that was authorized by the Rockefeller University Institutional Animal Care and Use Committee. Mice were randomized based on age and weight. Before treatment, we ensured that the mean weight and age were comparable among the various treatment groups.

## Statistical analysis

Results from multiple experiments are presented as mean  $\pm$  s.e.m. One- or two-way ANOVA was used to test for differences in the mean values

of quantitative variables, and where statistically significant effects were found, post hoc analysis using Bonferroni (adjusted for multiple comparisons) test was performed. A two-tailed t-test was used to test for differences in datasets with two groups. Statistical differences between survival rates were analyzed by comparing Kaplan-Meier curves using the long-rank (Mantel-Cox) test. Data were analyzed with GraphPad Prism v.10.2 software (GraphPad) and  $P < 0.05$  were considered to be statistically significant. For statistical analysis of DMS data we used two-sided Fisher’s exact test, followed by Bonferroni correction.

## Reporting summary

Further information on research design is available in the Nature Portfolio Reporting Summary linked to this article.

## Data availability

The crystallographic data of complex CU43<sup>D187A-D189A-Fc $\epsilon^{382S}$</sup>  generated in this study including atomic coordinates and structure factors have been deposited in the Protein Data Bank database under accession code **8URO**. The raw protein mass spectrometry data generated in this study are provided in the Supplementary Data file. Accession codes used in this study: CU43<sup>D187A-E189A</sup> (PDB code: **8UEN**), Fc IgG1 (PDB code: **5JH**), FcγRIIA-Fc (PDB code: **1E4K**), C1q-Fc (PDB code: **6FCZ**), IdeS-Fc (PDB code: **8A47**), ProteinA-Fc (PDB code: **5U4Y**), Protein G-Fc (PDB code: **1FCC**), FcRn-Fc (PDB code: **7Q15**), TRIM 21-Fc (PDB code: **2IWG**) and EndoS-Fc (PDB code: **8A64**), EndoS2-Fc (PDB code: **8Q5U**). Sequences and data related to DMS assays were deposited in NCBI BioProject: PRJNA1263835, NCBI, Biosample (SAMN48540644) and BioSample (SAMN48540644). Mass spectrometry data are provided in the Supplementary Data file. Source data are provided with this paper.

## Code availability

Original codes are available in ([https://github.com/Ortlund-Laboratory/DMS\\_EndoS2 CU43\\_CM49/tree/main/Deposited\\_Data/ CU43/Snakemake\\_Input](https://github.com/Ortlund-Laboratory/DMS_EndoS2 CU43_CM49/tree/main/Deposited_Data/ CU43/Snakemake_Input)) <https://doi.org/10.5281/zenodo.15446472> and ([https://github.com/Ortlund-Laboratory/DMS\\_IgG1Fc/tree/main](https://github.com/Ortlund-Laboratory/DMS_IgG1Fc/tree/main)).

## References

1. Fairbanks, A. J. The ENGases: versatile biocatalysts for the production of homogeneous N-linked glycopeptides and glycoproteins. *Chem. Soc. Rev.* **46**, 5128–5146 (2017).
2. Trastoy, B. et al. Structural basis of mammalian high-mannose N-glycan processing by human gut *Bacteroides*. *Nat. Commun.* **11**, 899 (2020).
3. Sastre, D. E. et al. Human gut microbes express functionally distinct endoglycosidases to metabolize the same N-glycan substrate. *Nat. Commun.* **15**, 5123 (2024).
4. Seki, H. et al. Structural basis for the specific cleavage of core-fucosylated N-glycans by endo-beta-N-acetylglucosaminidase from the fungus *Cordyceps militaris*. *J. Biol. Chem.* **294**, 17143–17154 (2019).
5. Collin, M. & Olsen, A. EndoS, a novel secreted protein from *Streptococcus pyogenes* with endoglycosidase activity on human IgG. *EMBO J.* **20**, 3046–3055 (2001).
6. Garcia-Alija, M. et al. Modulating antibody effector functions by Fc glycoengineering. *Biotechnol. Adv.* **67**, 108201 (2023).
7. Abes, R. & Teillaud, J. L. Impact of glycosylation on effector functions of therapeutic IgG. *Pharm. (Basel)* **3**, 146–157 (2010).
8. Naegeli, A. et al. *Streptococcus pyogenes* evades adaptive immunity through specific IgG glycan hydrolysis. *J. Exp. Med.* **216**, 1615–1629 (2019).
9. Trastoy, B. et al. Crystal structure of *Streptococcus pyogenes* EndoS, an immunomodulatory endoglycosidase specific for human IgG antibodies. *Proc. Natl. Acad. Sci. USA* **111**, 6714–6719 (2014).

10. Klontz, E. H. et al. Molecular basis of broad spectrum N-glycan specificity and processing of therapeutic IgG monoclonal antibodies by endoglycosidase S2. *ACS Cent. Sci.* **5**, 524–538 (2019).

11. Trastoy, B. et al. Mechanism of antibody-specific deglycosylation and immune evasion by Streptococcal IgG-specific endoglycosidases. *Nat. Commun.* **14**, 1705 (2023).

12. Sudol, A. S. L., Butler, J., Ivory, D. P., Tews, I. & Crispin, M. Extensive substrate recognition by the streptococcal antibody-degrading enzymes IdeS and EndoS. *Nat. Commun.* **13**, 7801 (2022).

13. Sudol, A. S. L., Crispin, M. & Tews, I. The IgG-specific endoglycosidases EndoS and EndoS2 are distinguished by conformation and antibody recognition. *J. Biol. Chem.* **300**, 107245 (2024).

14. Trastoy, B. et al. Sculpting therapeutic monoclonal antibody N-glycans using endoglycosidases. *Curr. Opin. Struct. Biol.* **72**, 248–259 (2022).

15. Wilson, M. J., Brandon, M. R. & Walker, J. Molecular and biochemical characterization of a protective 40-kilodalton antigen from *Corynebacterium pseudotuberculosis*. *Infect. Immun.* **63**, 206–211 (1995).

16. Shadnezhad, A., Naegeli, A. & Collin, M. CP40 from *Corynebacterium pseudotuberculosis* is an endo-beta-N-acetylglucosaminidase. *BMC Microbiol.* **16**, 261 (2016).

17. Sastre, D. E. et al. Potent efficacy of an IgG-specific endoglycosidase against IgG-mediated pathologies. *Cell* **187**, 6994–7007 (2024).

18. Keith, A. D. et al. Mapping affinity and allostery in human IgG antibody Fc region-Fc gamma receptor interactions. Preprint at bioRxiv <https://doi.org/10.1101/2025.03.28.645945> (2025).

19. Abramson, J. et al. Accurate structure prediction of biomolecular interactions with AlphaFold 3. *Nature* **630**, 493–500 (2024).

20. Alderson, T. R., Pritisanac, I., Kolaric, D., Mosecs, A. M. & Forman-Kay, J. D. Systematic identification of conditionally folded intrinsically disordered regions by AlphaFold2. *Proc. Natl. Acad. Sci. USA* **120**, e2304302120 (2023).

21. Tunyasuvunakool, K. et al. Highly accurate protein structure prediction for the human proteome. *Nature* **596**, 590–596 (2021).

22. Ultsch, M., Braisted, A., Maun, H. R. & Eigenbrot, C. 3-2-1: Structural insights from stepwise shrinkage of a three-helix Fc-binding domain to a single helix. *Protein Eng. Des. Sel.* **30**, 619–625 (2017).

23. Sauer-Eriksson, A. E., Kleywegt, G. J., Uhlen, M. & Jones, T. A. Crystal structure of the C2 fragment of streptococcal protein G in complex with the Fc domain of human IgG. *Structure* **3**, 265–278 (1995).

24. Brinkhaus, M. et al. The Fab region of IgG impairs the internalization pathway of FcRn upon Fc engagement. *Nat. Commun.* **13**, 6073 (2022).

25. James, L. C., Keeble, A. H., Khan, Z., Rhodes, D. A. & Trowsdale, J. Structural basis for PRYSPRY-mediated tripartite motif (TRIM) protein function. *Proc. Natl. Acad. Sci. USA* **104**, 6200–6205 (2007).

26. Sondermann, P., Huber, R., Oosthuizen, V. & Jacob, U. The 3.2-A crystal structure of the human IgG1 Fc fragment-Fc gammaRIII complex. *Nature* **406**, 267–273 (2000).

27. Ugurlar, D. et al. Structures of C1-IgG1 provide insights into how danger pattern recognition activates complement. *Science* **359**, 794–797 (2018).

28. Nandakumar, K. S. et al. Endoglycosidase treatment abrogates IgG arthritogenicity: importance of IgG glycosylation in arthritis. *Eur. J. Immunol.* **37**, 2973–2982 (2007).

29. Albert, H., Collin, M., Dudziak, D., Ravetch, J. V. & Nimmerjahn, F. In vivo enzymatic modulation of IgG glycosylation inhibits autoimmune disease in an IgG subclass-dependent manner. *Proc. Natl. Acad. Sci. USA* **105**, 15005–15009 (2008).

30. Collin, M., Shannon, O. & Bjork, L. IgG glycan hydrolysis by a bacterial enzyme as a therapy against autoimmune conditions. *Proc. Natl. Acad. Sci. USA* **105**, 4265–4270 (2008).

31. Merchant, A. M. et al. An efficient route to human bispecific IgG. *Nat. Biotechnol.* **16**, 677–681 (1998).

32. van Zundert, G. C. P. et al. The HADDOCK2.2 web server: user-friendly integrative modeling of biomolecular complexes. *J. Mol. Biol.* **428**, 720–725 (2016).

33. Zhang, C., Shine, M., Pyle, A. M. & Zhang, Y. US-align: universal structure alignments of proteins, nucleic acids, and macromolecular complexes. *Nat. Methods* **19**, 1109–1115 (2022).

34. Greaney, A. J. et al. Complete mapping of mutations to the SARS-CoV-2 spike receptor-binding domain that escape antibody recognition. *Cell Host Microbe* **29**, 44–57.e9 (2021).

35. Zhao, H., Brautigam, C. A., Ghirlando, R. & Schuck, P. Overview of current methods in sedimentation velocity and sedimentation equilibrium analytical ultracentrifugation. *Curr. Protoc. Protein Sci. Chapter* **20**, 12 (2013).

36. Zhao, H. et al. A multilaboratory comparison of calibration accuracy and the performance of external references in analytical ultracentrifugation. *PLoS One* **10**, e0126420 (2015).

37. Dam, J. & Schuck, P. Calculating sedimentation coefficient distributions by direct modeling of sedimentation velocity concentration profiles. *Methods Enzymol.* **384**, 185–212 (2004).

38. Rambo, R. P. & Tainer, J. A. Characterizing flexible and intrinsically unstructured biological macromolecules by SAS using the Porod-Debye law. *Biopolymers* **95**, 559–571 (2011).

39. Petoukhov, M. V. et al. New developments in the ATSAS program package for small-angle scattering data analysis. *J. Appl. Crystallogr.* **45**, 342–350 (2012).

40. Svergun, D. I., Petoukhov, M. V. & Koch, M. H. Determination of domain structure of proteins from X-ray solution scattering. *Bioophys. J.* **80**, 2946–2953 (2001).

41. Tuukkanen, A. T., Kleywegt, G. J. & Svergun, D. I. Resolution of ab initio shapes determined from small-angle scattering. *IUCrJ* **3**, 440–447 (2016).

42. Du, J. J. et al. Mass Spectrometry-Based Methods to Determine the Substrate Specificities and Kinetics of N-Linked Glycan Hydrolysis by Endo-beta-N-Acetylglucosaminidases. *Methods Mol. Biol.* **2674**, 147–167 (2023).

43. Johnson, K. A., Simpson, Z. B. & Blom, T. Global kinetic explorer: a new computer program for dynamic simulation and fitting of kinetic data. *Anal. Biochem* **387**, 20–29 (2009).

44. DiLillo, D. J., Tan, G. S., Palese, P. & Ravetch, J. V. Broadly neutralizing hemagglutinin stalk-specific antibodies require Fc gammaR interactions for protection against influenza virus in vivo. *Nat. Med.* **20**, 143–151 (2014).

45. Smith, P., DiLillo, D. J., Bournazos, S., Li, F. & Ravetch, J. V. Mouse model recapitulating human Fc gamma receptor structural and functional diversity. *Proc. Natl. Acad. Sci. USA* **109**, 6181–6186 (2012).

46. Bournazos, S., Corti, D., Virgin, H. W. & Ravetch, J. V. Fc-optimized antibodies elicit CD8 immunity to viral respiratory infection. *Nature* **588**, 485–490 (2020).

47. Tamura, K., Stecher, G. & Kumar, S. MEGA11: molecular evolutionary genetics analysis version 11. *Mol. Biol. Evol.* **38**, 3022–3027 (2021).

## Acknowledgements

We would like to thank SER-CAT APS (USA) Beamline ID-22 APS. Research reported in this publication was supported in part by the National Institute of Allergy and Infectious Diseases Grants R01AI149297 (to E.J.S), R01AI137276 (to S.B.), U19AI111825 (to J.V.R.), by National Institute of Biomedical Imaging and Bioengineering of the National Institutes of Health grant 3U54EB027690 (to E.A.O), by the National Cancer Institute grant R01CA244327 (to S.B.) and by the MICINN/FEDER EU grant PID2021-122177NA-I00 (to B.T.). BT was supported by a “Ramón y Cajal” fellow. Mass Photometry data was acquired on Refeyn Two<sup>MP</sup> mass

photometer funded by NIH 1R01GM148075-01 (to E.J.S). The content is solely the responsibility of the authors and does not necessarily represent the official views of the NIH.

## Author contributions

Conceptualization: D.E.S, S.B, J.V.R and E.J.S; Methodology, D.E.S, S.B, B.A.C.G., E.J.B, M.H, J.D, N.S, T.A, T.B, M.W.F, P.L, T.X, T.A.C, A.D.K, M.K, A.M.G, B.T, M.E.G, F.F, E. A.O, J.V.R, E.J.S; Investigation: D.E.S, M.H, B.A.C.G., E.J.B, J.D, N.S, T.A, T.B, M.W.F, P.L, T.X, A.S, T.A.C, A.D.K, M.K, A.M.G, B.T, F.F; Data Curation, D.E.S, A.D.K; Writing—Original Draft: D.E.S and E.J.S; Writing—Review & Editing: D.E.S, S.B, E.J.B, A.D.K, J.V.R and E.J.S.; Funding Acquisition: S.B, B.T, E.A.O, J.V.R and E.J.S; Resources: S.B, J.V.R and E.J.S; Supervision: D.E.S, S.B, E.O, J.V.R and E.J.S.

## Competing interests

D.E.S., S.B, J.D, J.V.R. and E.J.S. are inventors on a provisional patent application filed with the United States Patent and Trademark Office by Emory University relevant to the work in this manuscript. All other authors declare they have no competing interests.

## Additional information

**Supplementary information** The online version contains supplementary material available at <https://doi.org/10.1038/s41467-025-60986-w>.

**Correspondence** and requests for materials should be addressed to Diego E. Sastre or Eric J. Sundberg.

**Peer review information** *Nature Communications* thanks the anonymous, reviewer(s) for their contribution to the peer review of this work. A peer review file is available.

**Reprints and permissions information** is available at <http://www.nature.com/reprints>

**Publisher's note** Springer Nature remains neutral with regard to jurisdictional claims in published maps and institutional affiliations.

**Open Access** This article is licensed under a Creative Commons Attribution-NonCommercial-NoDerivatives 4.0 International License, which permits any non-commercial use, sharing, distribution and reproduction in any medium or format, as long as you give appropriate credit to the original author(s) and the source, provide a link to the Creative Commons licence, and indicate if you modified the licensed material. You do not have permission under this licence to share adapted material derived from this article or parts of it. The images or other third party material in this article are included in the article's Creative Commons licence, unless indicated otherwise in a credit line to the material. If material is not included in the article's Creative Commons licence and your intended use is not permitted by statutory regulation or exceeds the permitted use, you will need to obtain permission directly from the copyright holder. To view a copy of this licence, visit <http://creativecommons.org/licenses/by-nc-nd/4.0/>.

© The Author(s) 2025